Model compounds for monitoring surface reactivity in the gas phase

by

Tanner R. Thiessen

Bachelor of Science (Honours), University of British Columbia, 2020

A THESIS SUBMITTED IN PARTIAL FULFILLMENT OF

THE REQUIREMENTS FOR THE DEGREE OF

MASTER OF SCIENCE

in the

DEPARTMENT OF CHEMISTRY

THE UNIVERSITY OF VICTORIA

Model compounds for monitoring surface reactivity in the gas phase

by

Tanner R. Thiessen

Bachelor of Science (Honours), University of British Columbia, 2020

Dr. J. Scott McIndoe (Department of Chemistry)

Supervisor

Dr. Dave Berg (Department of Chemistry)

Supervisory Committee Member

Dr. John Burke (Department of Biochemistry and Microbiology)

External Examiner

Abstract

Atomic Layer Deposition (ALD) is a cyclic process in which volatile precursors are reacted with a surface to generate a single layer of atoms or molecules and this process can be repeated to tune the thickness of these layers. Currently ALD is used in the manufacturing of silicon-based semiconductors, but the process faces reactivity issues that hinder its efficiency. A new set of precursors of the form $X_3SiCo(CO)_4$ have been proposed to fix these reactivity issues. In order to study the mechanistics of this process, analysis of the interaction between the $X_3SiCo(CO)_4$ compounds and the surface must be observed. Due to heterogeneity of the surface and the small number of atoms involved model systems can be a powerful tool to better understand the chemistry occurring at the surface.

The model system chosen for this experiment is a compound called silsesquioxane that mimics the silicon surfaces reactivity, but also is available in the aqueous form. The experiment will be analyzed using electrospray ionization mass spectrometry (ESI-MS) coupled with a sample acquisition technique called pressurized sample infusion (PSI). These techniques were chosen because of their ability to handle highly air- and moisture-sensitive compounds as well as their ability to acquire data in real time. In order for mass spectrometry to be used, the precursors had to be charged and this was done by reacting the precursors with phosphine charged tags which generated charged analogues of the ALD precursors.

These techniques were also used in a collaboration project to examine the reduction of bis(cyclopendadienyl)titanium(IV) dichloride (Cp_2TiCl_2) with manganese dust in dry THF with the manual addition of deoxygenated water. This reaction undergoes colour change from the initial red titanium species to the green reduced species and finally deep blue once the deoxygenated water is introduced to solution. ESI-MS was used at each of these colour changes to observe the reaction intermediates and help elucidate the reaction mechanism.

Table of Contents

List of Tables

List of Figures

List of Schemes

List of Abbreviations

ALD = Atomic layer deposition

BPP = Benzylbis(diphenylphosphino)ethane

PPN = Bis(triphenylphosphine)iminium

CID = Collision induced dissociation

DFT = Density functional theory

DC = Direct-current

ESI = Electrospray Ionization

HAT = Hydrogen atom transfer

PF_6 = Hexafluorophosphate

HPLC = High-performance liquid chromatography

IR = Infrared

MS = Mass spectrometry

Ph = Phenyl

PSS = Polyhedral silsesquioxane

PEEK = polyetheretherketone

PTFE = polytetrafluoroethylene

PSI = Pressurized sample infusion

RF = Radio frequency

RBF = Round bottom flask

SET = single-electron transfer

MS/MS = Tandem mass spectrometry scans

CCTBA = *tert*-(butylacetylene)dicobalt hexacarbonyl

THF = Tetrahydrofuran

TPPMS = Triphenylphosphinomonosulfonate

TQD = Triple quadrupole

Acknowledgements

First and foremost, I would like to thank Prof. Scott McIndoe for initially seeing something valuable in me and for giving me the opportunity to complete my master's at UVic in an incredible group. Also, for his endless assistance and patience with my many questions and issues throughout the duration of my degree. I can not stress enough how enjoyable my time was working under Dr. Mcindoe's guidance.

I would like to thank my committee for their assistance in completing this program and for giving me guidance and helping me learn throughout the years.

I would like to thank the friends I had coming into UVic and the friends I made during my stay there. There were times during this program that were extremely difficult for me due to world issues and circumstances, and I truly wouldn't have been able to preserver and complete this degree without the endless assistance and companionship from them.

I'd like to thank my incredible undergraduate assistants Tiago Fisher and Jaspreet Sidhu. They worked exceptionally hard for me and it was a pleasure to work alongside them.

Finally, I'd like to thank my family for always being there for me and supporting me in everyway possible, whether it be random stops by my house to drop off much needed dinners during writing or to always be the best version of myself.

Dedication

“The darkest hour is just before the dawn”

-Tanner Thiessen

He knew this because of all the hours he spent doing lab work and writing until the sun came up in the morning.

1 Background

Portions of this chapter have been adapted from A. Joshi, C. Killeen, T. Thiessen, H.S. Zijlstra, J.S. McIndoe “Handling considerations for the mass spectrometry of reactive organometallic compounds”, *Journal of Mass Spectrometry*, **2022**, *57* (3), 1–15. Literature review and writing was collaboratively done by all authors.

1.1 Mass Spectrometry

The first instrument to separate ions by mass-to-charge ratio (*m/z*) was constructed by Joseph John Thomson thus creating the basis for mass spectrometry (MS).[1] Since its inception, mass spectrometry has undergone massive changes but the fundamental principles remain the same. A mass spectrometer consists of an ion source, a mass analyzer, and a detector which are operated under high vacuum conditions.[1] Ions are generated at the ion source, travel through the mass analyzer causing separation by electric and magnetic fields based on their *m/z*, and get detected at the detector. A spectrum of abundance or intensity versus *m/z* can then be obtained from these detections.

Mass spectrometry is an indispensable analytical tool in chemistry, biochemistry, pharmacy, medicine, and many related fields of science.[1] Its low limits of detection, unequalled sensitivity, speed and diversity of application have made it a staple instrument in most laboratories.[2] Mass spectrometry applications range from use in sequencing biomolecules[3] to analyzing atmospheric samples of other planets.[4]

In order for an analyte to be detected using mass spectrometry, the sample must be charged. This can occur using either a hard or soft ionization method. The hard ionization methods cause significant fragmentation as the ionization process typically requires a lot of energy which breaks the molecule apart, making it difficult to observe the signal for the whole molecule. Where soft ionization methods typically cause little to no fragmentation to occur, allowing for the whole molecule of interest to be observed. For use in this thesis, we require a soft ionization method in order to evaluate the mechanism of reaction between whole molecules and that wouldn’t be possible with a hard ionization method. One soft ionization method of interest is electrospray ionization (ESI).

1.1.1 Electrospray Ionization

ESI was first introduced in 1968 by Malcom Dole[5] and later was popularized as one of the most used ionization methods for mass spectrometry after significant innovations by John Fenn.[6,7]

ESI uses electrical energy to assist the transfer of ions from solution into the gaseous phase before they are subjected to mass spectrometric analysis.[8] Samples are introduced through a charged stainless steel capillary, typically between 2 to 5kV. Sample acquisition can be done either in positive or negative ion mode. For positive ion mode, the capillary is positively charged and in negative ion mode the capillary is negatively charged. Since analytes must be charged in order to be monitored using mass spectrometry, the analytes can either be charged by the solution or have inherent charges on the molecule. Acidic solutions are used to charge analytes for positive ion mode analysis and basic solutions are used for negative ion mode analysis.

The transfer of charged analytes from solution into the gas phase by ESI involves three steps: dispersal of a fine spray of charged droplets, followed by solvent evaporation, and ion ejection from the highly charged droplets.[7,8] The charged solution experiences a charged field as it is expelled from the capillary which causes the separation of charges and the formation of a Taylor cone (see **Figure 1.1**). Charged droplets are released from the Taylor cone and travel towards the mass analyzer. The charged droplets experience desolvation at this stage, aided by a desolvation gas (typically N_2), which increases the surface charge density of the droplets as the radius of the droplets decrease. Charged molecules are expelled from the droplets into the gas-phase as Coulombic repulsion exceeds surface tension.[7] These charged molecules are drawn into the mass spectrometer by electric fields and reduced pressure.

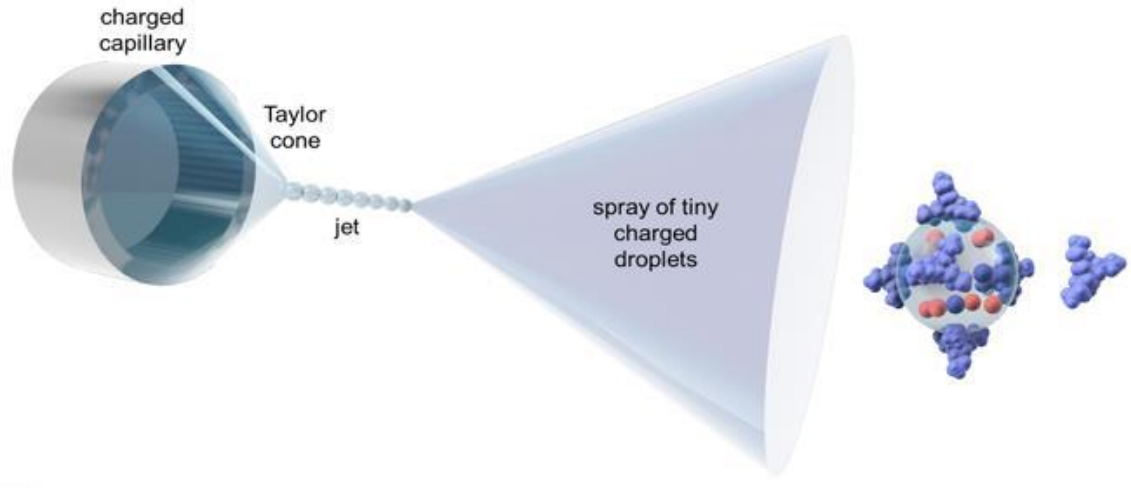

Figure 1.1: Electrospray Ionization (ESI).

1.1.2 Triple Quadrupole Mass Analyzer

Once the ions have been generated, they need to flow through a mass analyzer before they can be allowed to enter the detector. ESI sources are often coupled with a triple quadrupole (TQD) mass analyzer. A quadrupole consists of four equally spaced cylindrical electrodes mounted in parallel in a square configuration (see **Figure 1.2**).[9] The electric field used to control the ions is generated by coupling opposite pairs of rods together and applying radio frequency (RF) and direct-current (DC) potentials between pairs.[9] Two of these rods opposite each other are positively charged and the other two are negatively charged. The ions are accelerated along the z axis entering the space between the quadrupole rods and they maintain their velocity along this axis.[2] Some ions are said to have unstable trajectories and these ions are lost, such as ions that have collided with an electrode. Ions that have successfully made it through the analyzer are said to possess stable trajectories, and these are able to be detected. Neutral molecules are lost as they enter the mass analyzer because they are unaffected by the field and cannot make it through the analyzer. If only RF is applied, ions of all *m/z* will be transmitted to the detector. If RF and DC are both applied, only the ions with a *m/z* that have a stable trajectory in the analyzer resulting in the transmission and collection of ions of a single *m/z*. In this way the TQD mass analyzer works as a mass filter.[9]

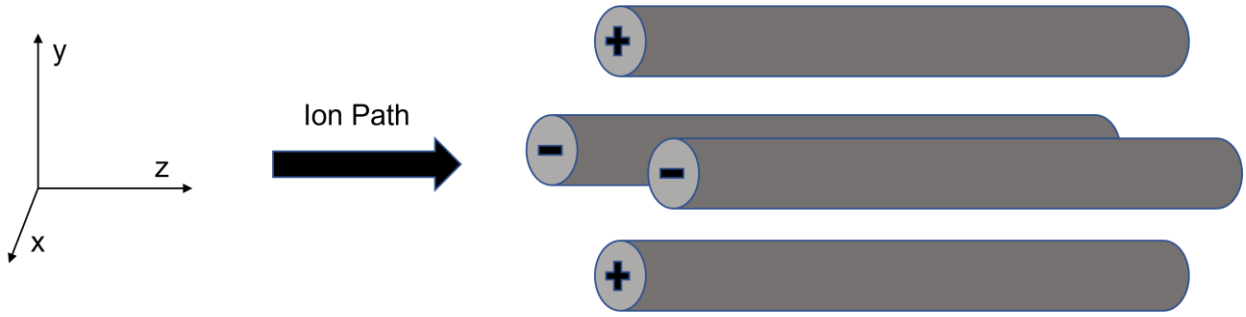

Figure 1.2: Depiction of the path an ion travels through a quadrupole mass analyzer with voltages displayed on the charged electrodes of the quadrupole

A TQD consists of three quadrupoles in succession arranged as Q1 followed by q2 and lastly Q3, involving two quadrupole mass analyzers and one collision cell. Q1 and Q3 are typical quadrupoles that allow all ions of the selected *m/z* range to have stable trajectories as they are analyzed, q2 is a collision cell which only experiences RF potential.

1.1.2.1 Tandem Mass Spectrometry

Tandem mass spectrometry scans (MS/MS) are a main feature of the TQD mass analyzer. Ions that enter the collision cell of a TQD instrument experience collision induced dissociation (CID) caused by the ions colliding with inert gas, allowing for further analyses of the structural properties of these ions to be observed as the ions enter Q3.[2]

Several modes of analysis exist when using MS/MS, including product ion scans, precursor ion scans, and neutral loss scans. For product ion scans, a specific *m/z* is selected for Q1, fragmentation occurs in q2, and all *m/z* are recorded in Q3 (see **Figure 1.3a**). All fragments of a specific *m/*z ion in Q1 are seen in the resulting spectrum. This allows for further analysis of what fragments make up a specific *m/z* signal. Precursor ion scans involve Q1 transmitting all *m/z* ions into the collision cell, fragmentation then occurs in q2 and Q3 is set to only allow a specific *m/z* into the detector (see **Figure 1.3b**). Only the parent ion of the fragment selected in Q3 is displayed on the resulting spectrum. Neutral loss scans involve both Q1 and Q3 scanning the whole *m/z* range, but with a constant mass offset between the two.[2] Thus, for a mass difference *a*, when an ion of mass *m* passes through Q1, it undergoes fragmentation in q2 and enters Q3 to be scanned (see **Figure 1.3c**). Detection occurs if this ion has yielded a fragment ion of mass (*m* – *a*) when it leaves the collision cell.[2] For example, in chemical ionization the alcohol molecule loses a water molecule. This alcohol is only detected in a neutral loss scan if a neutral loss of 18 mass units is observed from the ion. For our uses, product ion scans will be used often to help identify product formation for our synthetic products.

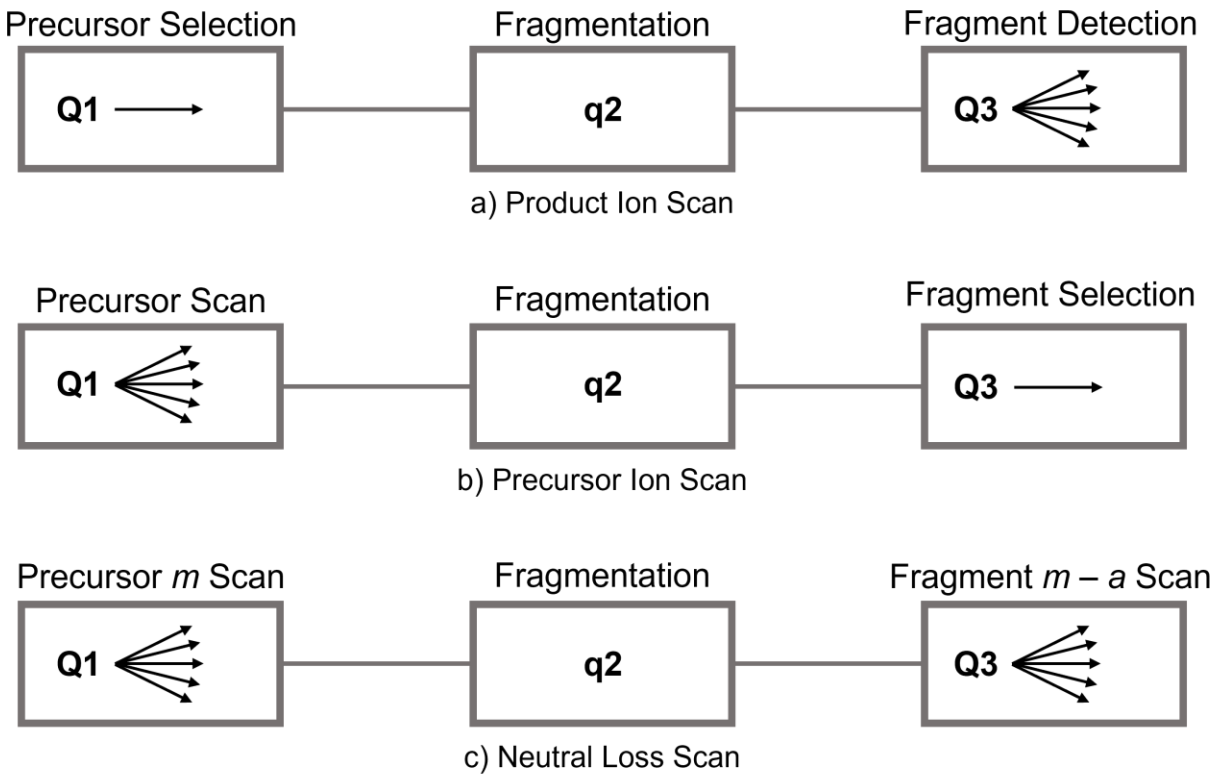

Figure 1.3: Schematic of (a) product ion scan; (b) precursor ion scan; and (c) neutral loss scan modes for a tandem mass spectrometer.[2]

1.1.3 Handling considerations for the mass spectrometry of reactive organometallic compounds

For the purposes of this thesis, a “reactive compound” is one that reacts in a deleterious way during routine mass spectrometric analysis. Mass spectrometry deals with very small amounts of material, so a compound that can survive brief exposure to the air as a bulk solid or as a concentrated solution may still appreciably decompose when exposed to oxygen and/or moisture as a few grains of material or a dilute solution. It is not always the case that the decomposition is obvious, either an oxidized ligand may decoordinate, a hydrolyzed product may oligomerize, or any number of other pathways may be unlocked. What these processes have in common is that they cause headaches for the analyst and the sample submitter alike. The procedures for handling these compounds all involve shielding the sample from exposure to air for even very brief periods and generally draw on standard laboratory procedures for handling reactive compounds.

ESI-MS is typically used on samples prepped in air but analysis of air- and moisture-

sensitive compounds can be achieved using a gastight syringe,[10] pressurized sample infusion (PSI),[11] or the more permanent solution of having a glovebox close to the mass spectrometer.[12] Analysis of highly reactive compounds also requires the use of exhaustively purified solvents. Solvents employed for ESI-MS of sensitive compounds are distilled and stored over activated molecular sieves for 3 days inside the glovebox before analysis.[13] Collecting spectra of extremely water-sensitive compounds can be negatively impacted by trace residual water from wet samples introduced to the instrument days, or even up to months beforehand. A good example is the $[Cp_2ZrMe]^+$ cation, which readily reacts with any residual water giving M + 2 species via $[M + H_2O - CH4]^+$ to produce $[Cp_2ZrOH]^+$. Trace amounts of water can complicate the analysis of methylalumoxane anions, as these anions can have dozens of Al-Me bonds, and multiple hydrolysis reactions could lead to very complicated spectra.

The collision gas also plays a significant role in getting reliable MS/MS spectra.[14] When the system being studied is very sensitive to air and moisture, such as $[Cp_2Zr(\mu\text{-}Me)_2AlMe_2]^+$ $[B(C6F5)4]^-$, the collision gas employed is often passed through a gas drying unit. However, moisture can also be in the collision chamber inside the mass spectrometer, which is very difficult to remove. Getting reliable MS/MS in such cases can be achieved by lowering the collision gas pressure.[14]

The desolvation gas employed for ESI-MS experiments is usually of very high purity (e.g., 99.995%). The effects of switching the desolvation gas source from a liquid N_2 dewar to an N_2 generator are reported in the literature.[14] Even for very reactive compounds, such as the reduced titanium complex $[Cp_2Ti(NCMe)_2]^+[ZnCl_3]^-$ and the olefin polymerization precatalyst $[Cp_2Zr(\mu\text{-}Me)_2AlMe_2]^+[B(C_5F_5)_4]^-$, very little oxidation was exhibited even when they were rendered coordinatively unsaturated through in-source fragmentation. Therefore, N_2 generators could be employed for analysis of organometallic compounds without significant concern over oxidation of the sample (the extent of oxidation was <4% at the highest flow rate = lowest purity N_2 examined).

Thoroughly rinsing the instrument before and after analysis is also necessary to avoid contamination from previous samples. While analyzing methylalumoxane, which is very sensitive to air and moisture, the source (i.e. sample cone and baffle) is rinsed periodically to prevent blockages (see **Figure 1.4**).

Figure 1.4: Baffle cone (top) before and Bottom after running methylalumoxane.

1.1.3.1 Pressurized Sample Infusion

Pressurized sample infusion is an easily implemented and low-cost solution to two problems organometallic chemists face in applying ESI-MS to their chemistry: how to analyze samples in an air- and moisture-free environment and how to continuously monitor reactions without the need for regular sampling, in any solvent and at any temperature.[11] This technique can be thought of as a cannula transfer from a Schlenk flask directly to the mass spectrometer. The PSI flask is designed to have an inlet where inert gas (Ar or N_2) is introduced, and this positive pressure allows the solution in the flask to be introduced to the mass spectrometer via PEEK/PTFE tubing.[15] Reactions can be conducted at temperatures up to the boiling point of the solvent, and the PSI flask is designed in a way that contamination from the rubber septum leaching from the solvent can be avoided entirely (see **Figure 1.5**).[16] PSI is straightforward to implement in any laboratory and allows continuous reaction monitoring in real time. PSI experiments can also be performed under the positive pressure of inert gas from a balloon instead of a gas cylinder.[17] This method of sample acquisition effectively limits the degradation of the reaction due to air and moisture.

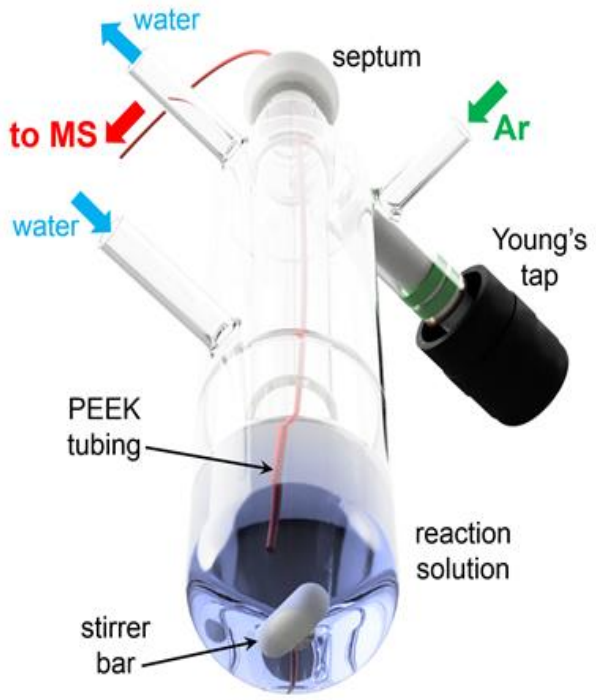

Figure 1.5: Pressurized sample infusion (PSI) flask.

PSI is ideal for the study of highly air-sensitive chemistry, exemplified by its use in the study of 1-hexene polymerization using a $Cp_2ZrCl_2/AlMe_3$ system. Using this technique, new pathways for catalyst deactivation, including the formation of dimethylalane-stabilized complexes, were identified.[18] PSI helped demonstrate how these complexes were resistant to further addition of hexene. The technique was used to study alkyl exchange in methylalumoxane, a very dynamic, fast, and difficult system to study.[19]

1.2 Objectives

The main goal of this thesis is to use ESI-MS and PSI–ESI–MS to elucidate mechanistic information and reactive intermediates in real time that would be difficult to impossible to acquire using other methods. These analytical techniques will be implemented using the air– and moisture–free techniques identified previously as all samples analyzed decompose rapidly and cannot be analyzed if either are introduced.

2 Model Systems for Atomic Layer Deposition (ALD) Processes using Mass Spectrometry

Conceptualization, proposal, and experimentation were chiefly completed by Tanner Thiessen. Undergraduate mentees Tiago Fisher and Jaspreet Sidhu assisted with experimentation and mass spectrometer acquisitions under the direct supervision of Tanner Thiessen. PhD candidate Sofia Donnecke assisted in the conceptualization and proposal of the project. Analysis of results and writing was done collaboratively by Tanner Thiessen and Scott McIndoe. Local company Seastar Chemicals, which manufactures organometallic precursors for atomic layer deposition (ALD) for use by the semiconductor industry, was also a collaborative partner. Seastar Chemicals is interested in developing better precursors that adhere cobalt selectively to silica surfaces. This research project was designed to examine the reactivity of silyl cobalt complexes for this purpose.

2.1 Abstract

A group of potential thermal Atomic Layer Deposition (ALD) precursors for deposition on silica were identified and studied using mass spectrometry. These precursors are of the form $X_3SiCo(CO)_4$ and were reacted with different charge-tagged phosphine ligands to create analogues of charged ALD precursors. The detailed syntheses of these compounds are detailed and preliminary investigations into their solution-phase reactivity described.

2.2 Introduction

Atomic Layer Deposition (ALD) is a gas phase thin film deposition technique that was first discovered in the 1960s.[20] This technique involves exposing the surface substrate to an alternating sequence of vapor phase reactants.[21] The reactants (known as precursors) react with the substrates in a self-limiting, thickness controlled fashion with high conformality.[22] Common reactants for ALD include, but are not limited to, trimethylaluminum (Me_3Al),[23] titanium tetrachloride ($TiCl_4$),[24] cobalt carbonyl ($Co_2(CO)_8$),[25] and bis(cyclopentadienyl)magnesium ($MgCp_2$).[26] All of these precursors have attractive characteristics for ALD in that they are volatile and decompose cleanly on surfaces by loss of their ligands as intact free molecules. These precursors usually (but not always) require a coreactant (sometimes called reductant), typically

hydrides such as H_2O and H_2S or non-hydride coreactants like O_2 in plasma enhanced ALD.[23,27] The full ALD cycle is illustrated in **Figure 2.1**.

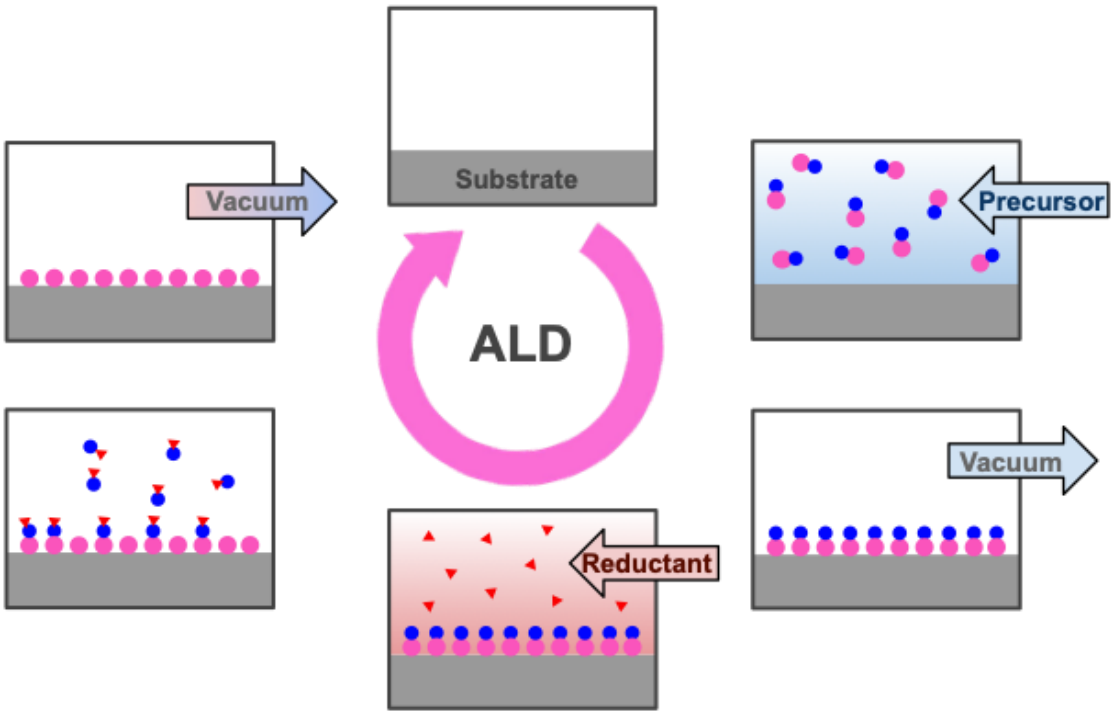

Figure 2.1: Visualization of the typical ALD process.

The cycle starts with a freshly cleaned substrate (top) in an air- and moisture-free environment, ready for the deposition process to begin. A precursor is introduced to the system that will react with the substrate to deposit itself in a molecular layer on top of the surface.[28] Once the surface is saturated, a vacuum removes excess precursors. These surface-bound reactants typically come with functional groups/ligands attached that allows them to react with just the surface and not with the incoming precursor. The new surface is treated with a reductant to generate a fresh new surface. Excess reductant and reduction byproducts are removed by application of heat and/or vacuum, leaving the surface with the precursor layer now exposed for further reactions in the ALD cycle. This new layer could be the same as the layer that was just added to build up the thickness and robustness of the layer (such as cobalt layered on itself) but can also be something entirely different to tune physical properties and/or reactivity (such as copper added above the cobalt layer).[29]

This generic ALD cycle is slightly more elaborate than what we will be discussing in our research, which is a simplified process called thermal ALD. This cycle is similar to the regular

ALD cycle except a reductant is not used (see **Figure 2.2**). Instead, after the first vacuum is pulled, the surface is heated (temperatures typically range between 150-350°C)[28] which causes all the ligands attached to the precursor to dissociate. A vacuum is applied to remove the dissociated ligands which generates a fresh surface without the need for a reductant. Thermal ALD is a feature of precursors where ligands can all be removed as neutral molecules (i.e. through ligand dissociation, e.g. CO, or reductive elimination, e.g. H_3CCH_3).

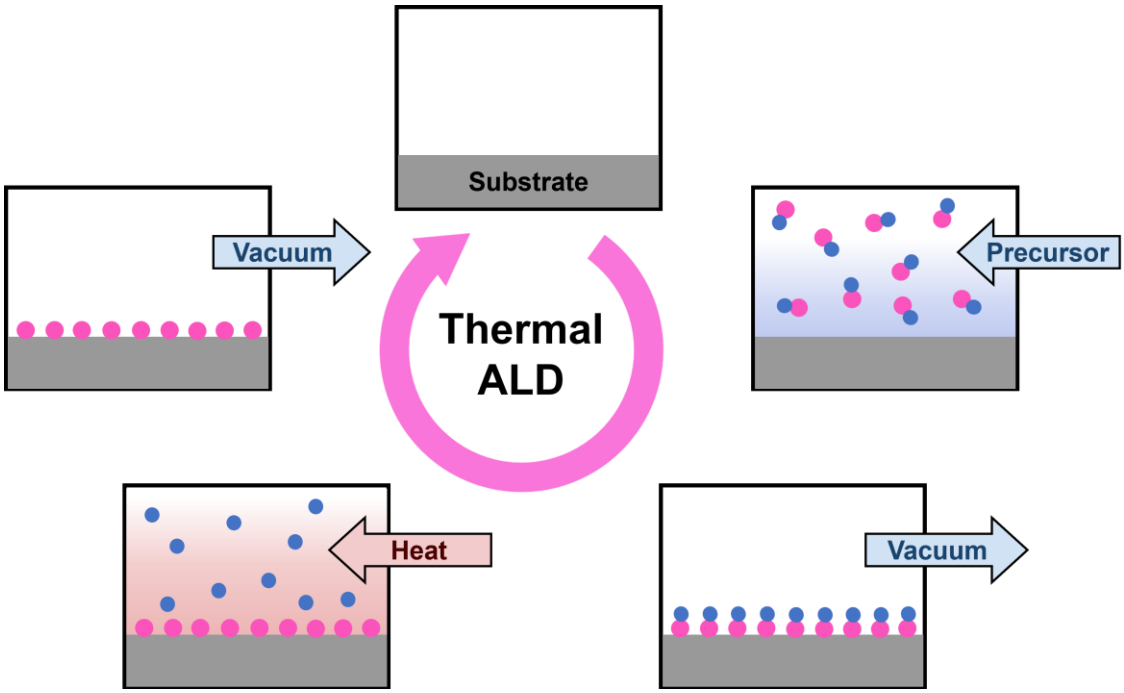

Figure 2.2: Visualization of the typical thermal ALD process.

ALD has had a variety of industrial uses over the years such as in photovoltaics[30], polymer surface functionalization[29] or use in thermo-optical coatings for spacecraft[31] but currently it is widely used in the manufacturing of semiconductors.[29] Semiconductors are comprised mostly of a single species of atom which are then doped with impurities to tune properties such as conductivity.[32] These single atom species are generally either silicon, germanium, tin, selenium or tellurium, but semiconductors are predominantly made from a silicon base (often doped with other elements to make *n*- and *p*-type semiconductors).[32,33] Patterned chips contain areas of semiconducting silicon and insulating areas made of silica (see **Figure 2.3**).[33]

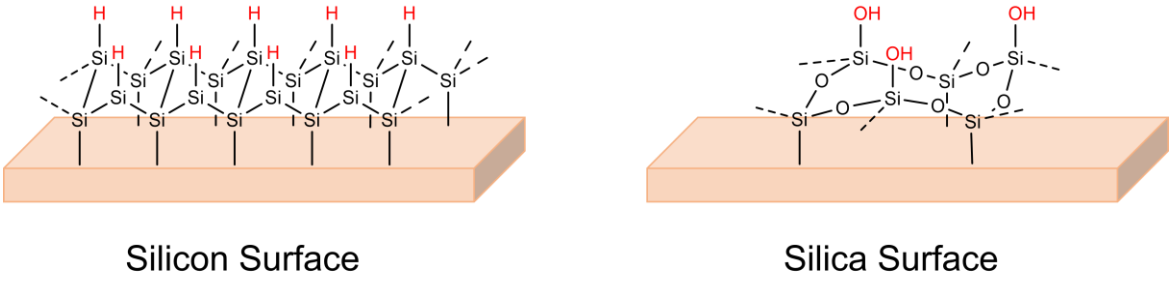

Figure 2.3: Visualizations of the Si-H terminated silicon surface (left) and the Si-OH terminated silica surface (right).

The silicon surface carries the charge that is passed through the device as it is used. The silica surface insulates the current so that the charge does not leak out of the system and is confined to the regions of the chip where it belongs. The reactivity of these surface layers is very different. The silicon surface is made up of a tight knit diamond-like structure with the top layer capped with hydrogen. However, close inspection of the silica surface shows that it is a more open lattice with bridging oxygen atoms woven between the silicon atoms and capped with silanol groups. Cobalt ALD on the silicon surface is well developed and typically occurs with cobalt carbonyl, $Co_2(CO)_8$, or with (*tert*-butylacetylene)dicobalt hexacarbonyl (CCTBA) (*tert*-butylacetylene = 3,3-dimethyl-1-butyne).[25] However, neither of these precursors allow for clean deposition of cobalt on the silica surface as they are unreactive towards the OH capped silica.[34] Consequently, we set out to design and synthesize compounds that would be selective for silic**a** surfaces over silic**on** surfaces. Such precursors would give chip makers the ability to layer cobalt on to either silicon or silica parts of the chip, granting them additional flexibility in design.

To do so, we opted to make silyl cobalt complexes of the form $X_3SiCo(CO)_4$, $MeX_2SiCo(CO)_4$ and $Me_2XSiCo(CO)_4$ (X = Ph, OMe, NMe_2, Cl) (see **Figure 2.4**), in order to add functional groups capable of forming new covalent bonds with the silica surface, adding a new Si-Co layer to the surface.

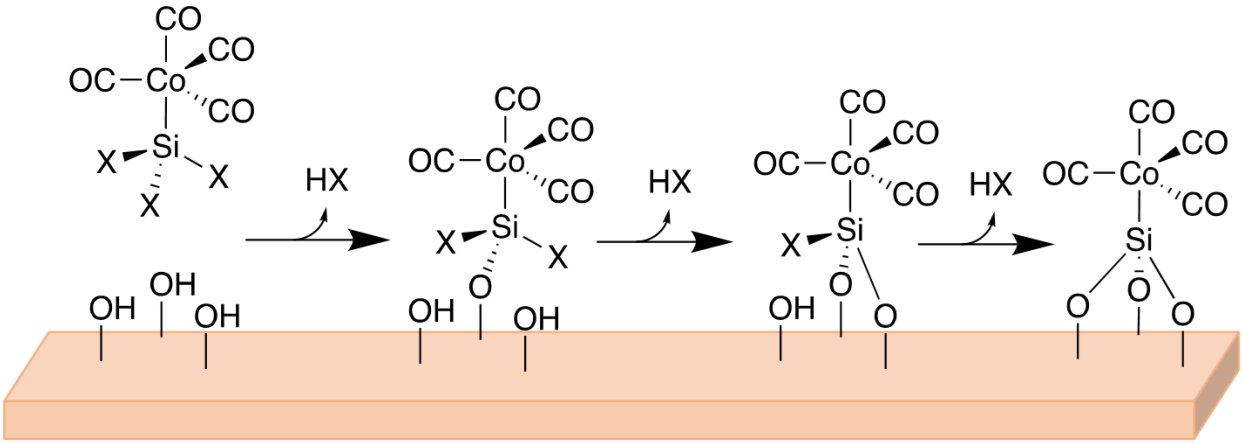

Figure 2.4: Proposed precursor undergoing deposition with the silica surface.

We believe that the silyl ligand will control the reactivity of the precursor with the surface, becoming integrated into the silica surface while remaining covalently bound to the cobalt, and presenting a surface layer of -$Co(CO)_4$ groups that can be stripped of carbonyl groups (via thermal ALD to remove the ligands as carbon monoxide) to leave cobalt atoms tenaciously bound to the silica surface, ready for a new round of ALD. Because the new surface will be very different from the previous one, the next precursor should be one with affinity for Co rather than Si-OH groups

The X groups on the silyl ligand can vary depending on the reactivity desired. Several potential silanes were identified for this deposition, triphenyl, trichloro, triethoxy, and tris(dimethylamino) silane (Ph_3SiH, Cl_3SiH, $(EtO)_3SiH$, $(Me_2N)_3SiH$). The first silane of interest was triphenyl silane. These other silane compounds are difficult to isolate due to their air- and moisture-sensitivity, but triphenyl silane has kinetically inert Si-C bonds that should allow it to be synthesized and isolated easily compared to the others. This precursor will not react with the silanols but is a good starting point to begin synthetic testing. Next, we looked to trichloro, triethoxy, and tris(dimethylamino) precursors, as these possess suitable reactivity with silanol groups. Additionally, we looked to isolate silyl cobalt species with different numbers of reactive X groups, such as dichloromethyl silane (Cl_2MeSi), to see how varying the number of reactive groups on the ligand influences the deposition of the precursor.

To study the molecular details of this process, we chose to further derivatize the cobalt centre with a charge-tagged phosphine ligand (see **Scheme 2.1**), thus enabling real-time analysis of the reactivity of these complexes and enabling examination of their unimolecular decomposition under elevated temperatures. The phosphine will most likely occupy the position *trans* to the silyl group for steric reasons (trigonal bipyramidal complexes are fluxional thanks to the Berry pseudo-rotation, so ligand exchange is facile).[35]

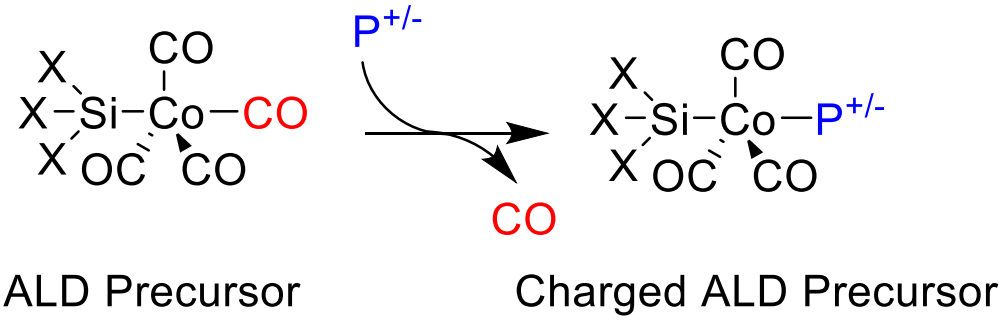

Scheme 2.1: Ligand exchange of the carbonyl group for an L type charged ligand.

Given that surface chemistry is generally difficult to monitor for mechanistic studies,[36] our reactions were done in solution with a surrogate of the silica surface sold as PSS-Trisilanol-isooctyl substituted ($C_{56}H_{122}O_{12}Si_7$, see **Figure 2.5**). This compound is a type of organosilicon compound called a silsesquioxane ("PSS" refers to polyhedral silsesquioxane), which featured many desirable qualities for our research. These compounds have a silica core with organic ligands attached to the outside. This silica core provides the compound with rigidity and thermal stability which aided us in our tests.[37] The silsesquioxane used mimics the spacing and silanol capped pieces of the silica surface, but it is soluble and of singular composition (unlike a surface), which made it amenable to our mass spectrometric techniques. For simplicity our compound is referred to as silsesquioxane throughout.

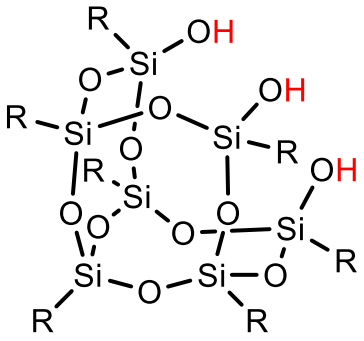

Figure 2.5: PSS-Trisilanol-isooctyl substituted (R = C_8H_{17}).

Mass spectrometric studies can be conducted by introducing the charged ALD precursor with silsesquioxane and monitoring the reactivity. As soon as the reaction begins, we expect to see a *m/z* change as the precursor initially binds to the silsesquioxane, generating HX in the process

(see **Scheme 2.2**). Then we will see how many silanol pieces react with the silyl cobalt precursor as the *m/z* ratio decreases with each subsequent exchange. This will help us identify the reactivity of our precursors as well as identify exactly how many silanol group will react with the precursor. We would assume that the initial binding will be slow as the precursor and silsesquioxane begin to interact, but the subsequent reactivity should be faster as the reactive groups on the silyl ligand are much closer to the other silanol sites once bound. At this stage we assume the reaction will go to completion and we will observe an increase in concentration of the triply bound silyl group as all available X are converted to HX.

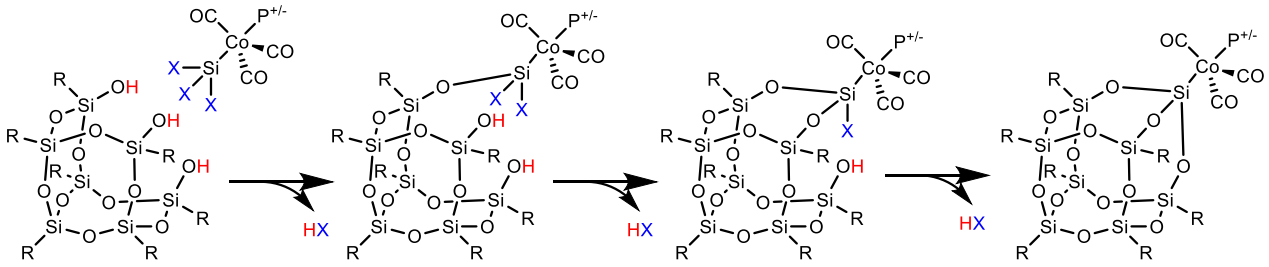

Scheme 2.2: Planned reaction of the charged ALD precursor with silsesquioxane.

2.3 Results and Discussion

To test the charged ALD precursors with silsesquioxane, we first had to synthesize the precursors as well as the charged precursors. Silyl cobalt complexes have been known for many years, and can be readily synthesized via reaction of a silane with $Co_2(CO)_8$.[38]

$$X_3SiH + 0.5\ Co_2(CO)_8 \longrightarrow X_3SiCo(CO)_4 + 0.5\ H_2\ (g) \qquad \textbf{Eqn. 1}$$

$$Co_2(CO)_8 \longrightarrow 2\ \cdot Co(CO)_4 \qquad \textbf{Eqn. 2}$$

$$X_3SiH + \cdot Co(CO)_4 \longrightarrow X_3Si\cdot + HCo(CO)_4 \qquad \textbf{Eqn. 3}$$

$$X_3Si\cdot + Co_2(CO)_8 \longrightarrow X_3SiCo(CO)_4 + \cdot Co(CO)_4 \qquad \textbf{Eqn. 4}$$

$$2\ HCo(CO)_4 \longrightarrow Co_2(CO)_8 + H_2\ (g) \qquad \textbf{Eqn. 5}$$

The overall reaction can be seen in **Eqn.** 1 with formation of one equivalent of the silyl cobalt precursor for one equivalent of silane to 0.5 equivalents of $Co_2(CO)_8$; 0.5 equivalents H_2 gas are released as a byproduct. This reaction seems quite simple but is actually a complex radical

mechanism. **Eqn. 2** shows the initiation of the reaction by homolytic cleavage of the Co-Co bond to make two $\cdot Co(CO)_4$ radicals. This radical reacts with the Si-H bond of X_3SiH to generate $HCo(CO)_4$ and $X_3Si\cdot$ (see **Eqn. 3**). The $X_3Si\cdot$ radical reacts with the Co-Co bond of the starting material $Co_2(CO)_8$ forming the desired compound $X_3SiCo(CO)_4$ and another equivalent of $\cdot Co(CO)_4$ (see **Eqn. 4**). The $HCo(CO)_4$ molecules can then combine to release H_2 and reform $Co_2(CO)_8$ (see **Eqn. 5**). This reaction works for a wide range of functional groups on silicon and is fast and high yielding. The products are reasonably volatile in most cases; impressively so in the case of $X_3Si = Cl_3Si$, where the product can be readily sublimed to rapidly form long pale-green needles (see **Figure 2.6**). Other examples are less volatile but often amenable to purification by the same technique.

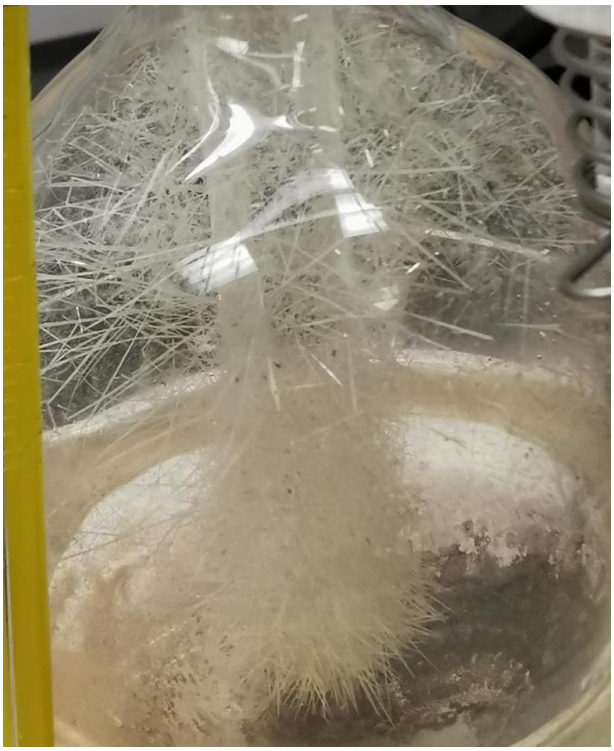

Figure 2.6: Sublimation of $Cl_3SiCo(CO)_4$ in a Schlenk flask contained initially in a N_2 atmosphere. Sublimation was completed over 2 h with static vacuum, a cold finger with cold water, and an oil bath held to 40°C.

The charged tag ligand requires an L-type (2 electron donor) ligand appended with a permanent charge. We chose to use a phosphonium-phosphine ligand, thanks to the synthetic convenience of these compounds, which are readily prepared by monoalkylation of a bisphosphine ligand (See **Eqn. 6**).[39]

$$R_2P(CH_2)_nPR_2 + R'Br \longrightarrow [R_2P(CH_{2)2}PR_2R']^+[Br]^- \qquad \textbf{Eqn. 6}$$

The halide counterion can be straightforwardly exchanged for a less coordinating anion such as $[PF_6]^-$, and we took this precaution when making our chosen ligand (R = Ph, n = 2, R' = $PhCH_2$, **1**).

There are two possible routes to the desired charged precursors: appending the phosphine ligand first and the silyl ligand second, or vice versa, as seen in **Scheme 2.3.** We attempted both.

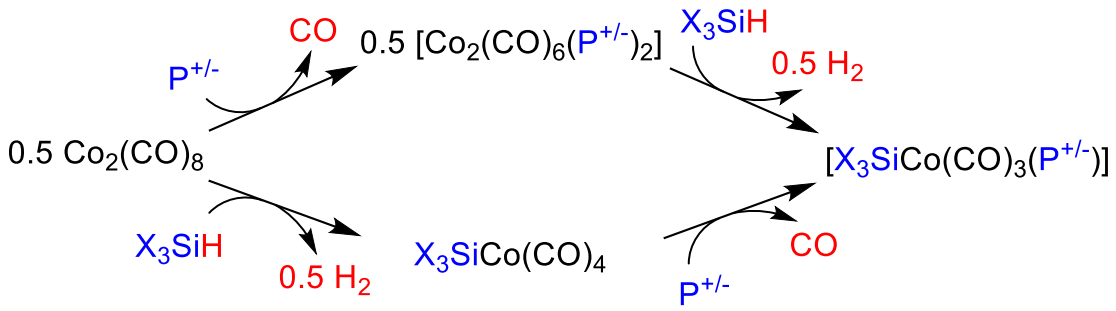

Scheme 2.3: Alternate routes to isolate the charged ALD precursors.

The first route involved addition of the phosphine ligand to $Co_2(CO)_8$ followed by homolytic cleavage of the Co-Co bond with X_3SiH. The phosphine was added to $Co_2(CO)_8$ in a 2:1 ratio, which produced the expected bis-substituted dimer (see **Eqn. 7**):

$$Co_2(CO)_8 + 2\ [\mathbf{1}][PF_6] \longrightarrow [Co_2(CO)_6(\mathbf{1})_2][(PF_6)_2] + 2\ CO \qquad \textbf{Eqn. 7}$$

This complex was fully characterized, including by X-ray crystallography (**Figure 2.7**). The structure is centrosymmetric and has the conventional geometry of $Co_2(CO)_6(PR_3)_2$ complexes, with the phosphine ligands *trans* to the Co-Co bond.[40] The complex has Co(1)-C(1/2/3) bond distances of 1.798(4) Å, 1.784(4) Å and 1.785(5) Å respectively, with a Co(1)-P(1) bond distance of 2.1848(10) Å. The carbonyls have C(1/2/3)-O(1/2/3) bond distances of 1.146(6) Å, 1.131(6) Å, and 1.142(5) Å respectively. Bond angles for C(1/2/3)-Co(1)-Co(1)#1 are 88.01(13)°, 87.78(13)°, and 81.38(13)° respectively, with a P(1)-Co(1)-Co(1)#1 bond angle of 173.25(4)°.

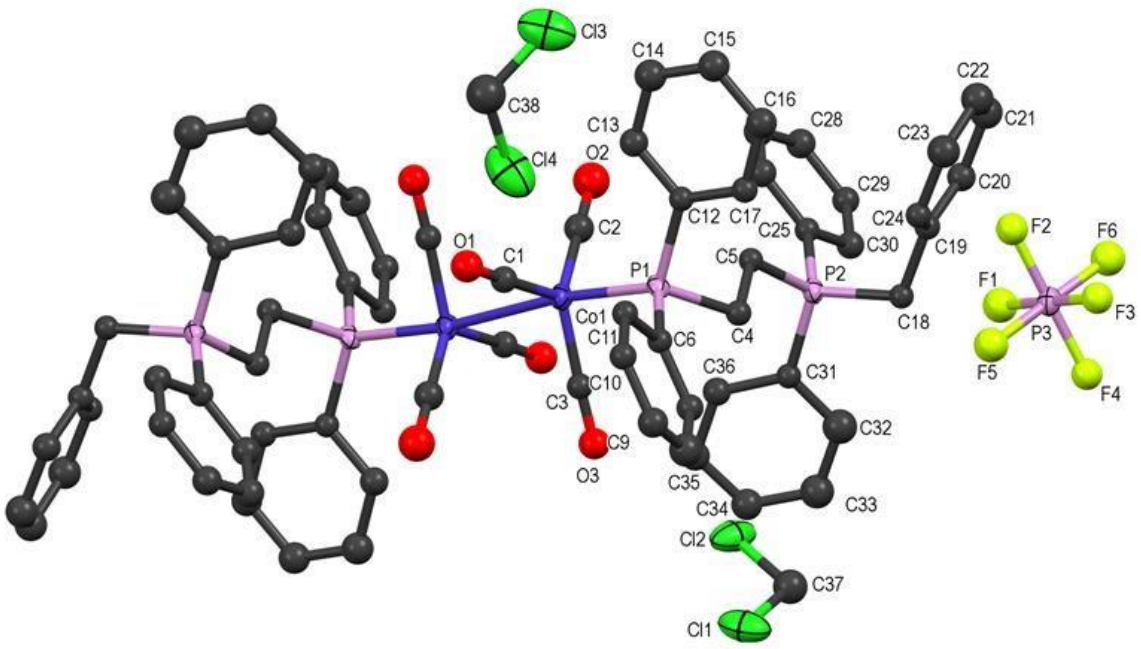

Figure 2.7: X-ray crystal structure of $[Co_2(CO)_6(\mathbf{1})_2][(PF_6)_2]$, with ellipsoids at the 60% level. The coordination geometry about each Co, including the Co-Co bond is trigonal bipyramidal, with the carbonyl ligands occupying equatorial positions and the phosphine ligand an axial position. The structure has two $[PF_6]^-$ anions and four molecules of CH_2Cl_2 trapped in its lattice. The second anion and two additional solvent molecules are omitted for clarity.

The positive ion mass spectrum of $[Co_2(CO)_6(\mathbf{1})_2]^{2+}$ featured the expected ion at *m/z* 632.5, with some free ligand present at *m/z* 489.0 and oxidized ligand at *m/z* 505.5 (see **Figure 2.8**). The calculated *m/z* for these ions are 632.1, 489.2 and 505.2 respectively. Even in rigorously anaerobic conditions, minimal amounts of oxygen can still be present in the MS as the sample is being run,[41] which caused our charged tag to become oxidized. MS/MS of the $[Co_2(CO)_6(\mathbf{1})_2]^{2+}$ ion resulted in fragmentation via loss of **1** as well as varying amounts of CO ligands.

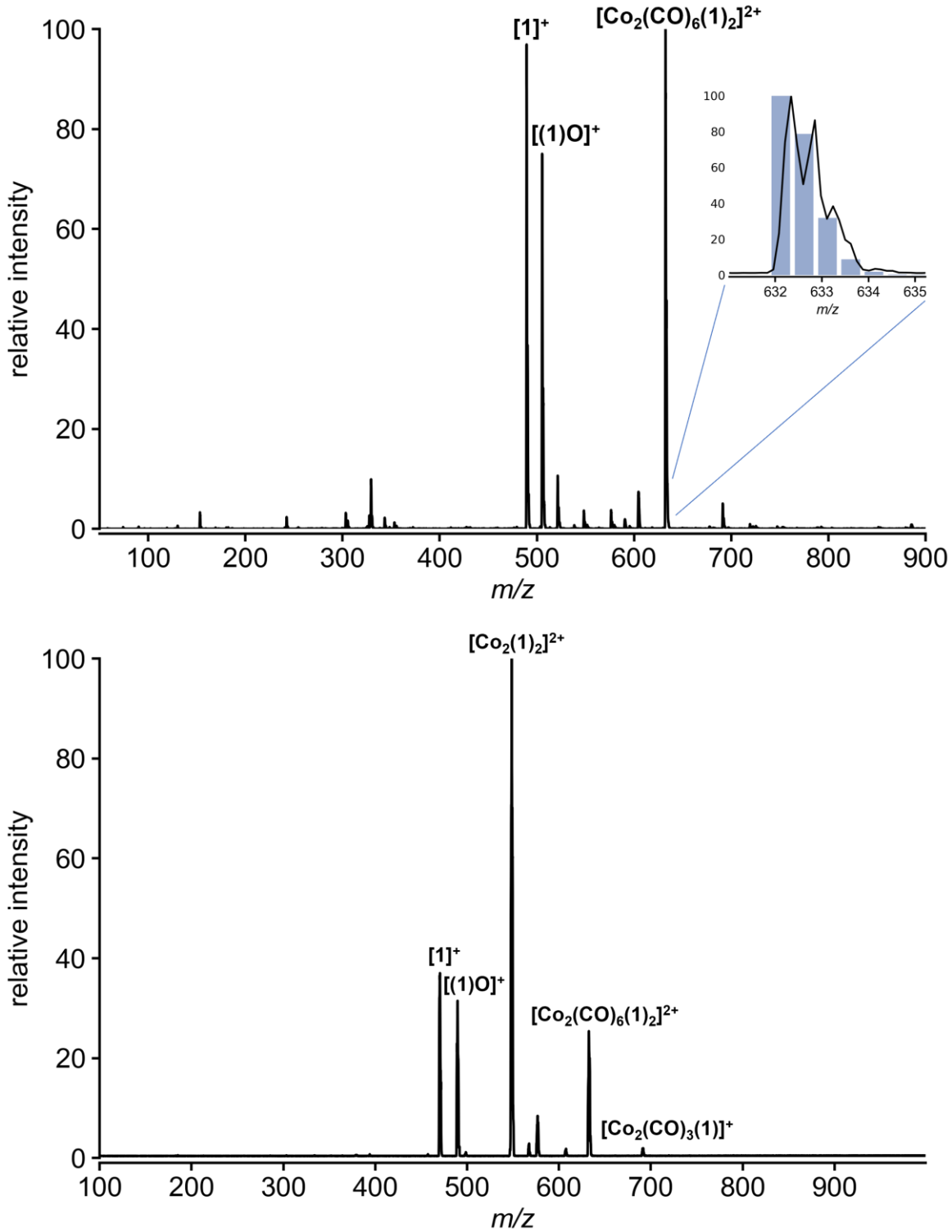

Figure 2.8: Positive ion mode mass spectrum of $[Co_2(CO)_6(\mathbf{1})_2]^{2+}$ (top) and a MS/MS spectrum acquired of the parent ion *m/z* 632.5 (bottom). The full spectrum has the calculated isotope pattern overlayed with the experimental spectrum acquired.

The charged precursor was obtained via addition of the silane to $[Co_2(CO)_6(\mathbf{1})_2][(PF_6)_2]$ (see **Eqn. 8**).

$$[Co_2(CO)_6(\mathbf{1})_2][(PF_6)_2] + 2\ X_3SiH \longrightarrow 2\ [X_3SiCo(CO)_3(\mathbf{1})][PF_6] + H_2 \quad \textbf{Eqn. 8}$$

This reaction proved to be difficult as $[Co_2(CO)_6(\mathbf{1})_2][(PF_6)_2]$ had low solubility in the solvents used and led to many decomposition products present when analysed on the MS. However, for the reaction of $[Co_2(CO)_6(\mathbf{1})_2][(PF_6)_2]$ with $(Me_2N)_3SiH$, the expected ion at *m/z* 792.5 was still observed with the correct isotope pattern and correlates closely to the calculated *m/z* of 792.2, as seen in **Figure 2.9**.

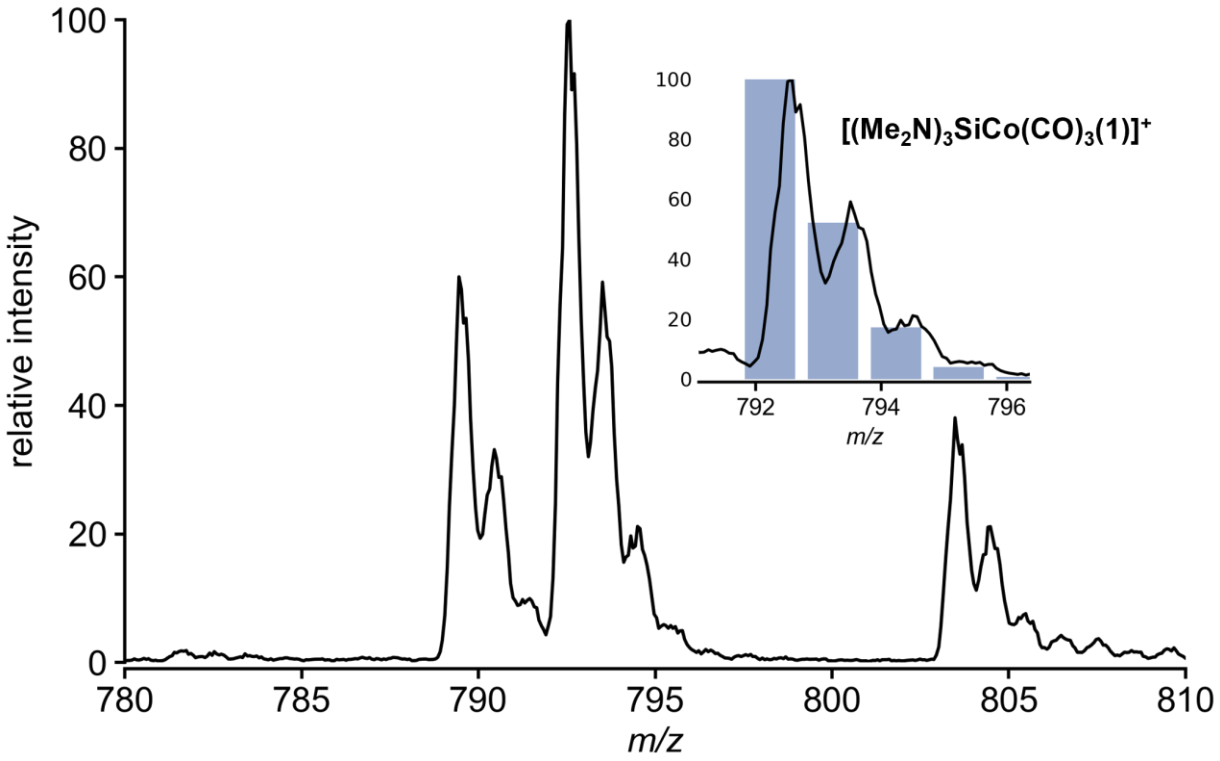

Figure 2.9: Positive ion mode ESI-MS of the products of the reaction of $(Me_2N)_3SiH$ with $[Co_2(CO)_6(\mathbf{1})_2][(PF_6)_2]$. The calculated isotope pattern has been overlayed on the experimental pattern.

Although the desired product was synthesized, the compound was not able to be isolated from solution. This was because of low product yield and high levels of decomposition being present. Due to these issues, this route was abandoned.

The second synthetic route was to first prepare the Si-Co bond, then substitute the charged tag (**1**) for a carbonyl ligand. The first step was the homolytic cleavage of the Co-Co bond to form the silyl cobalt precursors as outlined above in **Eqn. 1**. This method allowed for the synthesis of a variety of $X_3SiCo(CO)_4$ complexes to be isolated (X_3Si = Ph_3Si, Cl_3Si, Cl_2MeSi, and $ClMe_2Si$). None of these precursor complexes were amenable to ESI-MS analysis (since they lack a charged tag) but could be readily characterized by their infrared (IR) spectrum (see **Figure 2.10**) (characteristic peaks in the metal carbonyl stretching region due to the C_{3V}-symmetric $Co(CO)_4$ group) and were able to be purified by sublimation or crystallization.

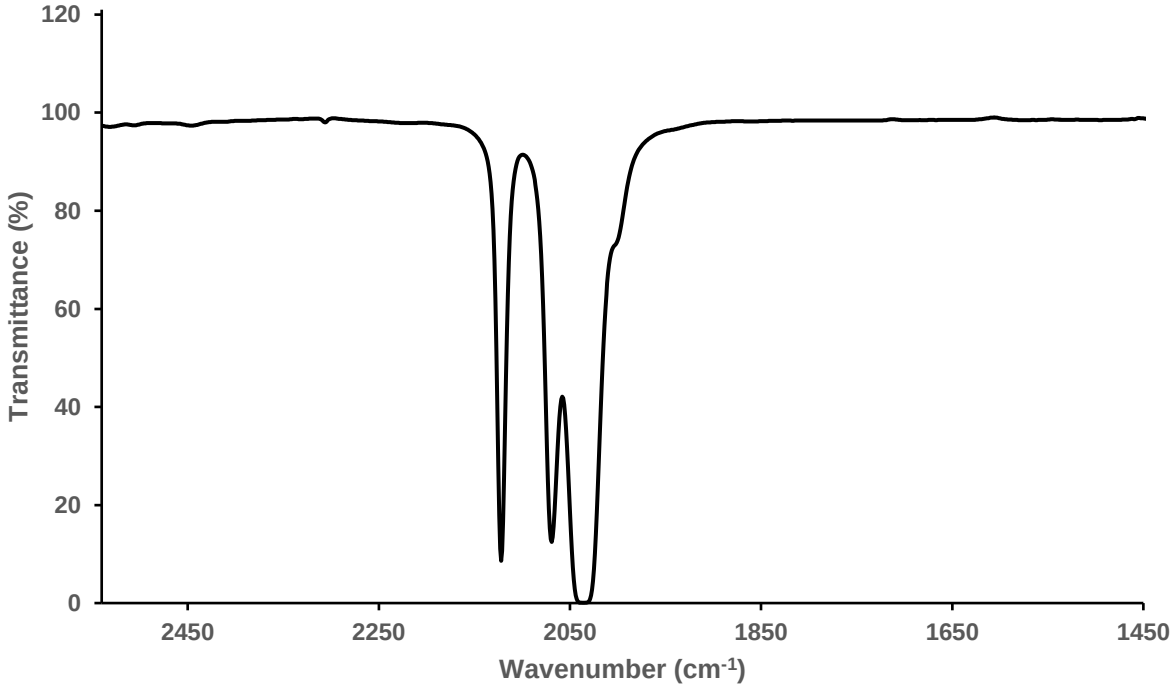

Figure 2.10: Solution cell IR spectrum displaying the carbonyl stretching region of $Cl_3SiCo(CO)_4$ in CH_2Cl_2. The peaks at 2122 cm^{-1}, 2069 cm^{-1}, and 2037 cm^{-1} align with literature C-O stretching values for this compound.[42] All $X_3SiCo(CO)_4$ compounds isolated followed this same stretching pattern except with slightly varied wavenumbers due to the different electronic properties of the ligands attached.

The charged precursor was then isolated following **Eqn. 9**

$$X_3SiCo(CO)_4 + [\mathbf{1}][PF_6] \longrightarrow [X_3SiCo(CO)_3(\mathbf{1})][PF_6] + CO \qquad \textbf{Eqn. 9}$$

Reaction of the $X_3SiCo(CO)_4$ compounds with a 1:1 ratio of **1**[PF_6] to $X_3SiCo(CO)_4$ resulted in the desired product in the case of X = Ph (see **Figure 2.11**).

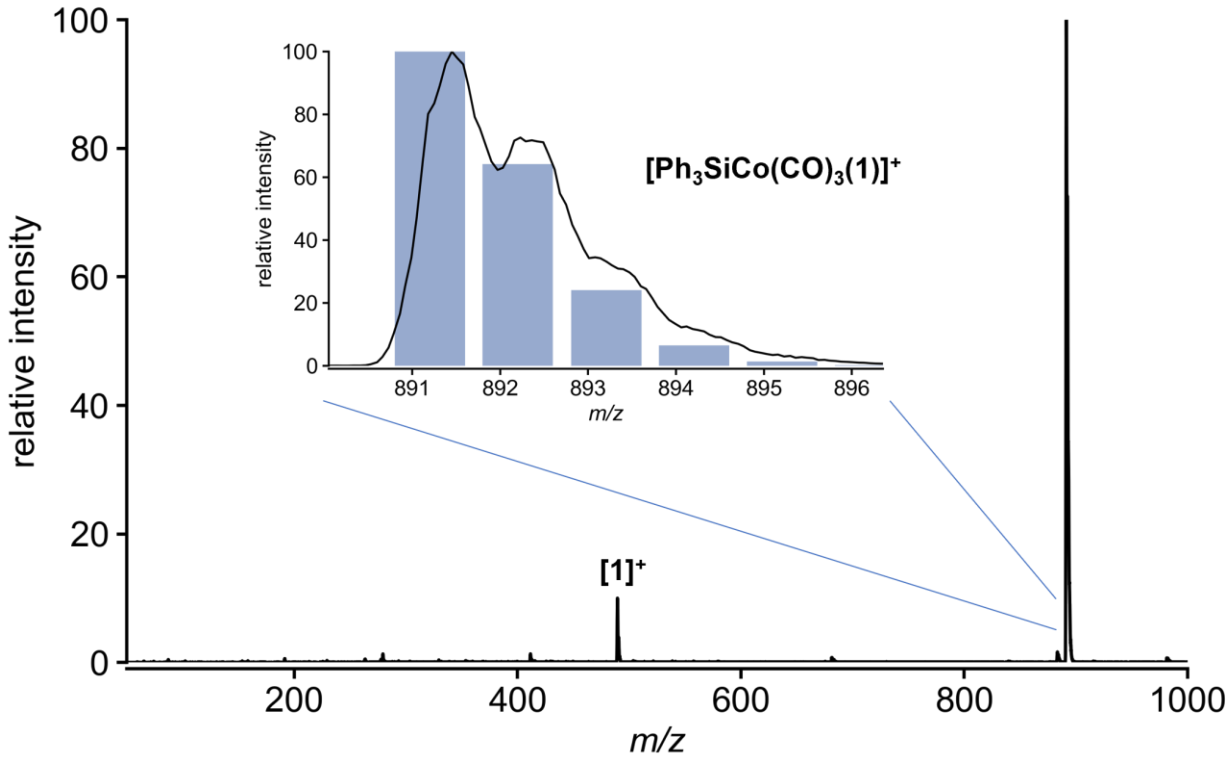

Figure 2.11: Positive ion mode mass spectrum of $[Ph_3SiCo(CO)_3(\mathbf{1})]^+$. The product ion and free ligand $[\mathbf{1}]^+$ are visible at *m/z* 891.5 and *m/z* 489.4 respectively with no other predominant ions present. The product ion has low resolution but the calculated isotope pattern with *m/z* of 891.2 and 489.2 has been matched to the experimental spectrum.

Although reaction of **1**[PF_6] with $Ph_3SiCo(CO)_4$ resulted in the charged precursor to be isolated, additional testing with the other precursors found that the most abundant charged product of these reactions was the doubly charged $[Co_2(CO)_6(\mathbf{1})_2]^{2+}$ and only minimal amounts of the desired $[X_3SiCo(CO)_3(\mathbf{1})]^+$ compounds were present in solution. This likely is caused by **1** binding *trans* to the silane bond, as seen in $[Co_2(CO)_6(\mathbf{1})_2]^{2+}$ with **1** binding *trans* to the Co-Co bond. This binding appears to be strong, which likely causes the Si-Co bond to weaken. Once weakened, the Si-Co bond likely homolytically cleaves creating $Ph_3Si\cdot$ and $\cdot[Co(CO)_3(\mathbf{1})]^+$. Then the cobalt radical reacts with itself to reform $[Co_2(CO)_6(\mathbf{1})_2]^{2+}$. Due to these issues, it was clear that a charged tag that would bind less strongly is required to form these species.

Having been unable to produce the desired compound, we turned to a triphenylphosphine monosulfonate charged tag called [TPPMS][PPN] (**2**[PPN], see **Figure 2.12**). This is a charged triphenylphosphine surrogate that was previously used by the McIndoe group.[43] This compound was similar in composition to **1**[PF_6] but the compound of interest will now be negatively charged rather than positively charged.

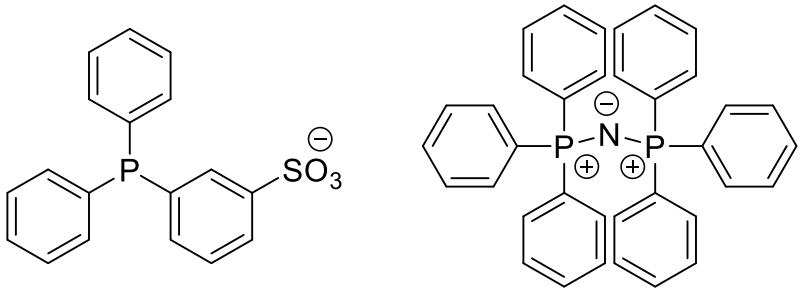

[TPPMS] [PPN]

Figure 2.12: Triphenylphosphinomonosulfonate (TPPMS) charged tag and its counter ion bis(triphenylphosphine)iminium (PPN).

2[PPN] was reacted with $X_3SiCo(CO)_4$ following **Eqn. 9** with the exception that **2**[PPN] was used in place of **1**[PF_6]. Reaction of **2**[PPN] with $Cl_3SiCo(CO)_4$ in a 1:1 ratio resulted in another charged precursor ($[Cl_3SiCo(CO)_3(\mathbf{2})]^-$) to be obtained in solution (see **Figure 2.13**).

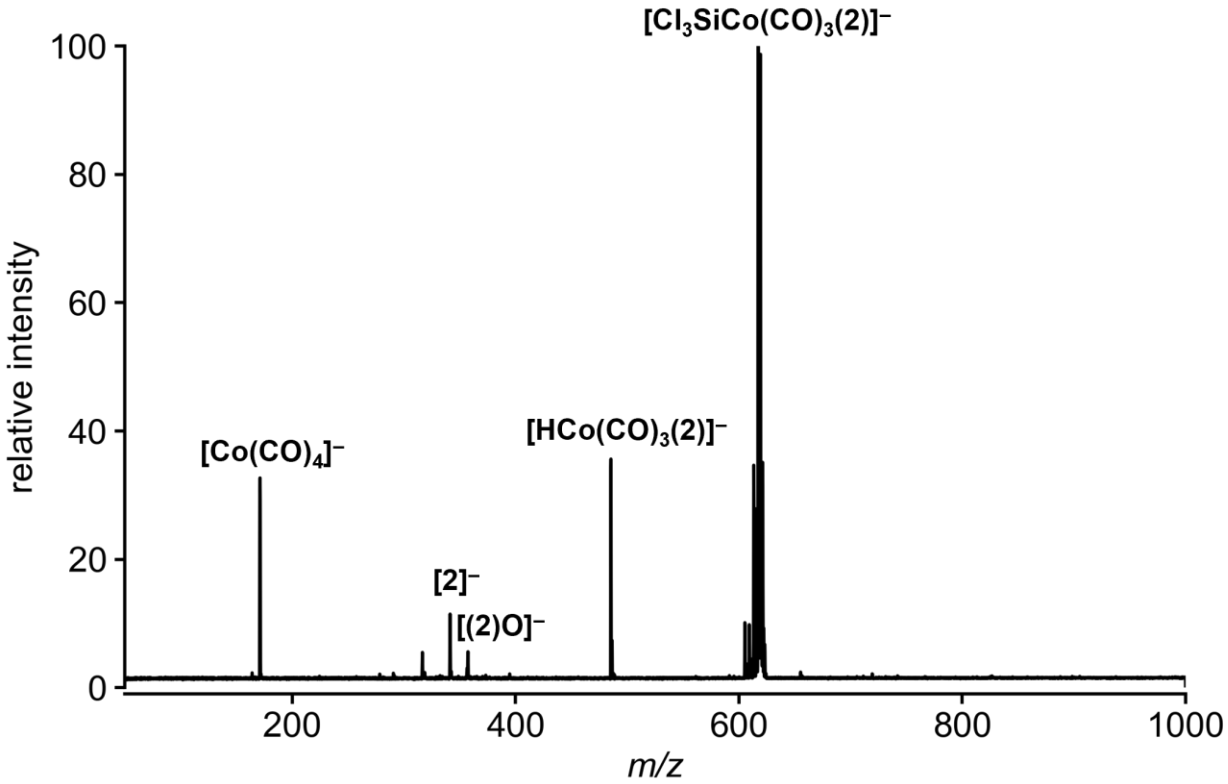

Figure 2.13: Negative ion mode mass spectrum of $[Cl_3SiCo(CO)_3(\mathbf{2})]^-$. The product ion is the predominant ion in the spectrum at *m/z* 617.2. Free ligand $[\mathbf{2}]^-$ and oxidized ligand visible at *m/z* 341.3 and *m/z* 357.4 respectively. Decomposition products $[Co(CO)_4]^-$ and $[HCo(CO)_3(\mathbf{2})]^-$ are observed at *m/z* 171.2 and *m/z* 485.2 respectively. These experimental signals corresponded to their respective calculated *m/z* of 616.8, 341.0, 357.0, 170.9 and 484.9.

The presence of the decomposition at *m/z* 171.2 corroborates our assumptions made to the decomposition of the neutral precursor as it interacts with our charged tags. It does appear though that the decomposition has been mitigated as our desired product has been obtained in a higher proportion to that of the decomposition. When investigating the parent ion of $[Cl_3SiCo(CO)_3(\mathbf{2})]^-$ there appeared to be some impurities present around it (see **Figure 2.14 (top)**). These impurities corresponded to $[Cl_2MeOSiCo(CO)_3(\mathbf{2})]^-$ (*m/z* 613.3) and $[Cl(MeO)_2SiCo(CO)_3(\mathbf{2})]^-$ (*m/z* 609.5). This meant the chlorines of $[Cl_3SiCo(CO)_3(\mathbf{2})]^-$ were likely exchanging with trace amounts of MeOH that was used to rinse the MS prior to acquisition. Another mass spectrum was obtained of $[Cl_3SiCo(CO)_3(\mathbf{2})]^-$ this time using CH_2Cl_2 as the rinsing solvent instead of MeOH (see **Figure 2.14 (bottom)**). No impurities were present around the parent ion showing that $[Cl_3SiCo(CO)_3(\mathbf{2})]^-$ must be able to exchange readily with MeOH.

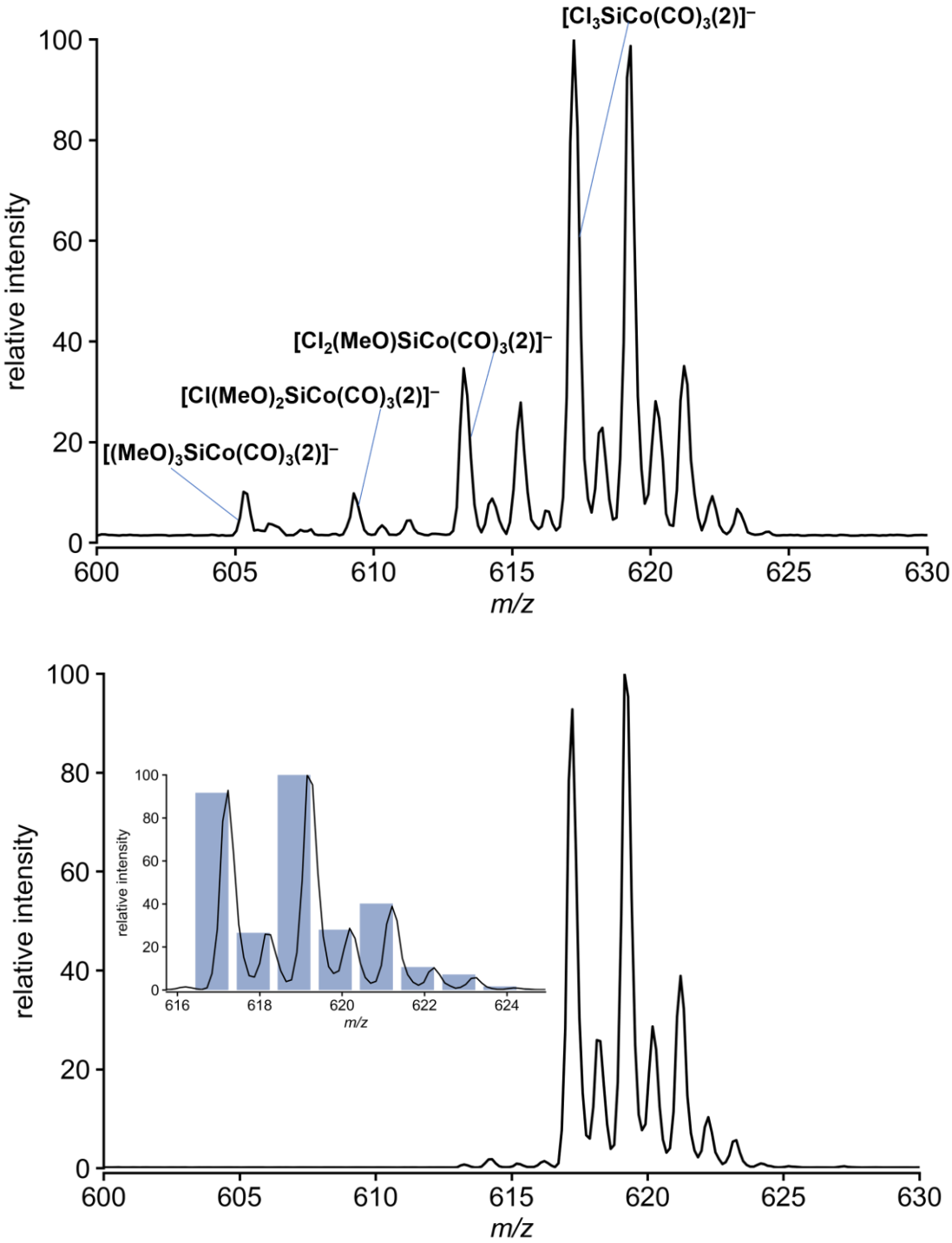

Figure 2.14: Negative ion mode mass spectra of the parent ion for $[Cl_3SiCo(CO)_3(\mathbf{2})]^-$ when changing the solvent used to rinse the ESI-MS, prior to acquisition, from MeOH (top) to CH_2Cl_2 (bottom). The bottom spectrum also has the calculated isotope pattern for $[Cl_3SiCo(CO)_3(\mathbf{2})]^-$ overlayed with the experimental spectrum.

To further test the alcohol exchanging capabilities of $[Cl_3SiCo(CO)_3(\mathbf{2})]^-$, it was then tested in a PSI-ESI-MS experiment with ethanol (see **Figure 2.15**). This reaction allowed for real time data of the reaction to be obtained when tracking each intermediate independently. This shows that the concentration of *m/z* 617.2 decreases throughout the course of the reaction as the first exchange of a chlorine for ethanol takes place. The concentration of *m/z* 627.3 increases rapidly at the start and slowly begins decreasing overtime as the second exchange occurs. The concentrations of *m/z* 637.3 and *m/z* 647.4 were both seen to increase overtime due to the time scale of this reaction, but it is assumed that given enough time the *m/z* 637.3 would start to decrease as more of it is converted to the fully exchanged $[(EtO)_3SiCo(CO)_3(\mathbf{2})]^-$ compound.

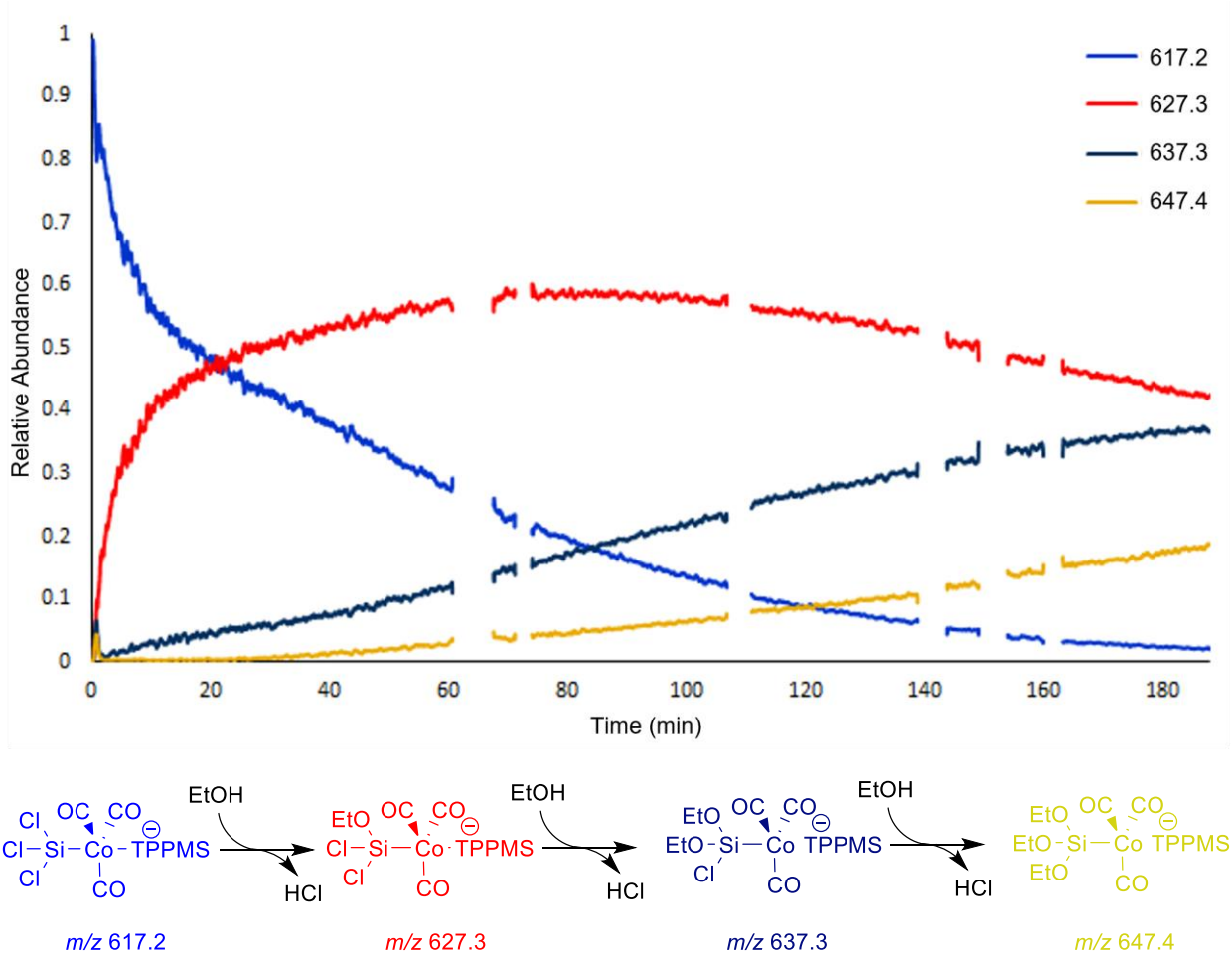

Figure 2.15: Real time reaction of $[Cl_3SiCo(CO)_3(\mathbf{2})]^-$ with EtOH monitored using PSI-ESI-MS. Throughout the course of the reaction the PEEK tubing would clog and all signals would be completely lost. This corresponds to the blank sections of the graph which were removed so the overall trend can be better visualized.

This data showed that $[Cl_3SiCo(CO)_3(\mathbf{2})]^-$ could exchange its chlorines without decomposition occurring and it was now ready to be tested with silsesquioxane. PSI-ESI-MS experiments were set up using the same sample that was used to create **Figure 2.15**, but the results were not as expected. We expected to see *m/z* 1763.6, *m/z* 1727.6, and *m/z* 1691.6, for the first, second, and third exchanges which corresponds to HCl being generated and the silane binding to the silanol of silsesquioxane. Instead, we observed many charged species that were close to the correct masses but were either a few mass units too high or too low. The most interesting signal was found at *m/z* 1800.0, seen in **Figure 2.16**.

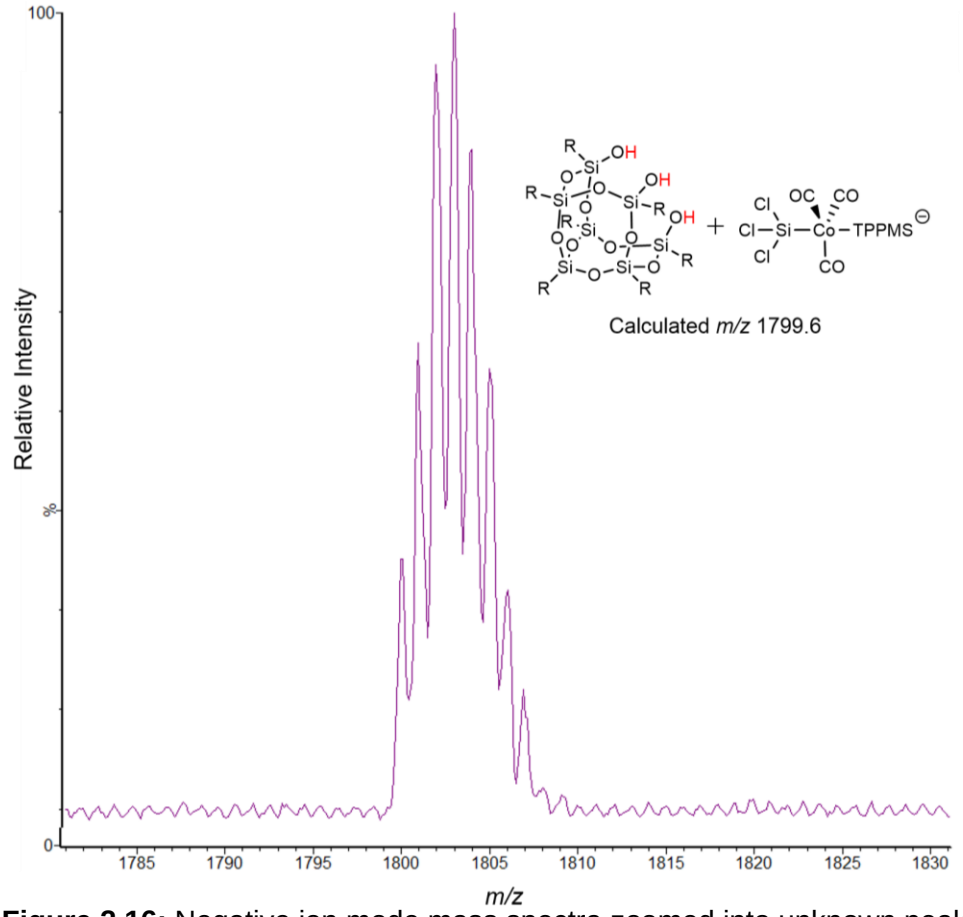

Figure 2.16: Negative ion mode mass spectra zoomed into unknown peak at *m/z* 1800.0 with its presumed ion overlayed.

This signal matches the signal that would be created if the silsesquioxane interacted with $[Cl_3SiCo(CO)_3(\mathbf{2})]^-$ but without loss of any HCl. MS/MS investigation of the signal at *m/z* 1800.0 further proved our hypothesis as it showed the *m/z* 617.2 starting material signal was one of the predominant ions after CID which meant the compound was interacting in some way with

silsesquioxane, but exchange did not appear to be occurring at this time. Potentially silsesquioxane was interacting with the charged sulfonate group of **2**. To rule this out, an experiment was conducted where the charged tag **2**[PPN] was reacted alone with silsesquioxane and monitored using PSI-ESI-MS. Data analysis of the reaction found no species of interest present during the reaction showing no interaction between the charged tag and silsesquioxane. This meant that silsesquioxane must be interacting with $[Cl_3SiCo(CO)_3(\mathbf{2})]^-$ to form an adduct but no elimination of HCl to form new Si-O bonds was observed. Further experimentation is required to establish the details of what is going on here, and we hope that our collaborations with computational chemists will help elucidate the nature of this interaction.

2.4 Conclusions

The syntheses and characterization of multiple $X_3SiCo(CO)_4$ (X = Cl, Ph, and Me_2N) and $Cl_NMe_MSiCo(CO)_4$ (N = 3 – M, M = 1 or 2) compounds was detailed above. The charged ALD precursors $[Cl_3SiCo(CO)_3(TPPMS)][PPN]$ and $[Ph_3SiCo(CO)_3(BPP)][PF_6]$ were also characterized and identified. $[Cl_3SiCo(CO)_3(TPPMS)][PPN]$ was reacted with MeOH and EtOH showing its capability to exchange its Cl with alcohol functional groups. $[Cl_3SiCo(CO)_3(TPPMS)][PPN]$ was reacted with silsesquioxane and showed an apparent interaction between the two but no binding was observed through successive loss of HCl. This interaction must be studied to identify the nature of the binding before further testing with silsesquioxane can be conducted.

2.5 Materials and Methods

All reagents and solvents were purchased from Sigma-Aldrich and used as received unless noted below. 4 Å molecular sieves were dried by heating them for 2 h via flame, under vacuum. Celite was dried by baking in an oven at 75°C for three days. High-performance liquid chromatography (HPLC)-grade dichloromethane (CH_2Cl_2) and methanol as well as reagent-grade hexanes were dried over CaH_2 then distilled onto dried 4 Å molecular sieves. Reagent-grade ethanol was dried over KOH then distilled onto dried 4 Å molecular sieves. All compounds that were dried were immediately stored under a nitrogen atmosphere in the glovebox.

The compounds used in these experiments were air and moisture sensitive so special considerations were made when handling these compounds for MS acquisition outside of the glovebox.[41] ESI-MS using a Waters Acquity Triple Quadrupole Detector equipped with a Z-Spray

electrospray ionization source was qualitatively used to confirm product isolation of all charged species in the positive or negative ion mode. Samples were loaded into a 1 mL plastic syringe in the glovebox. The syringe was connected to the MS with PEEK tubing. The capillary voltage was held at 3 kV, cone voltage at 15 V and the desolvation gas flow rate was 100 L/h, cone gas flow rate 100 L/h, source temperature 50°C and desolvation temperature 160°C. After each run, the MS was rinsed using methanol with the same voltages and flow rates, but the source and desolvation temperatures were 80°C and 200°C respectively. ESI-MS was also used to acquire the data for all PSI experiments using the same parameters. These experiments were conducted using a custom made Schlenk flask[16] and connected to the MS via PEEK tubing inserted through a rubber septum. At this time the flask would contain the charged species of interest in solution, under an argon atmosphere. The neutral species of interest was then injected into the solution, starting the reaction. All samples run on the mass spectrometer were dissolved in CH_2Cl_2. The mass spectrometer and PEEK tubing was then rinsed with HPLC-grade methanol until no discernable signal was present. The IR spectra acquired were run using a Perkin-Elmer Spectrum Two spectrometer. All spectra were acquired in air- and moisture-free environments as solution cells using CH_2Cl_2 as the solvent of choice.

2.6 Experimental

Unless otherwise noted, all reactions were carried out using standard Schlenk and glovebox techniques under rigorously anhydrous, anaerobic, nitrogen atmosphere. Cobalt carbonyl (≥90% moistened with hexanes) had large amounts of purple decomposition products present upon arrival and had to be purified using hexanes prior to use. This was done by dissolving the cobalt carbonyl in hexanes then gravity filtering the solution, leaving behind the insoluble purple impurity ($CoCO_3$). The solution was stored in the freezer for 1 day to crystallize out the cobalt carbonyl. This yielded pure cobalt carbonyl that was able to be stored in the glovebox freezer for months with no new decomposition forming (see **Figure 2.17**). [TPPMS][PPN] was previously synthesized by the McIndoe group[43] and was readily available for use. Filter pipettes (1.5 mL × 270 mm soda-lime glass Pasteur pipette plugged with a small amount of kimwipe and covered with 2 to 3 cm of celite) were used periodically to remove solid impurities from solution.

Figure 2.17: Cobalt carbonyl crystals that have been recrystallized and isolated from hexanes.

2.6.1 Charged Tag Syntheses

Benzylbis(diphenylphosphino)ethane bromide, [BPP][Br]

1,2-bis(diphenylphosphino)ethane (1.786 g, 4.483 mmol, 1 eq) was added to a 100 mL RBF in air. 20 mL of toluene was then added to the flask and gentle heating was used to fully dissolve the solid. Benzyl bromide (0.52 mL, 4.4 mmol, 1 eq) was then syringed into solution slowly over 1 min. The solution was left to react for 40 h after which the solution was chilled in an ice bath briefly before being vacuum filtered and washed twice with 10 mL of chilled toluene. The product was isolated as a soft white powder (2.185g, 88%); ESI-MS: $[BPP]^+$ *m/z* 489, $[Br]^-$ *m/z* 79.

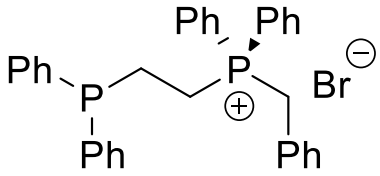

Benzylbis(diphenylphosphino)ethane hexafluorophosphate, [BPP][PF_6]

[BPP][Br] (2.000 g, 3.512 mmol, 1 eq) was added to a 100 mL beaker and dissolved in a minimal amount of hot methanol in air. Sodium hexafluorophosphate (0.667 g, 3.971 mmol, 1.1 eq) was dissolved in a minimal amount of hot deionized water in a 100 mL beaker. The sodium hexafluorophosphate solution was added dropwise to the [BPP][Br] solution with stirring. The solution was chilled for 10 min in an ice bath. The solution was vacuum filtered and washed twice

with 10 mL of chilled deionized water. The product was isolated as a sticky white powder (1.354 g, 61%); ESI-MS: $[BPP]^+$ *m/z* 489, $[PF_6]^-$ *m/z* 145.

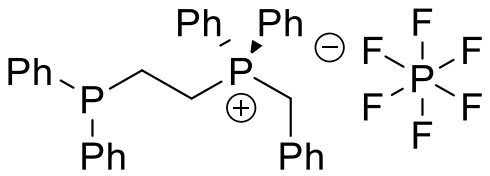

2.6.2 Silyl Cobalt Precursor Syntheses

Cobalt(tetracarbonyl)(triphenylsilyl), $Co(CO)_4(Ph_3Si)$

This compound was synthesized using a modified preparation.[44] Cobalt carbonyl (106.6 mg, 0.312 mmol, 1 eq) was added to a 100 mL Schlenk flask and dissolved in 5 mL hexanes. Triphenylsilane (174.0 mg, 0.668 mmol, 2.1 eq) was added to a glass vial and dissolved in 3 mL of hexanes. The triphenylsilane solution was added dropwise to the cobalt carbonyl solution. The solution was left to react for 2 h. Over the course of the reaction, the solution changed colour from reddish orange to dark purple with white precipitate present. The solution was concentrated to roughly 2 mL *in vacuo*. The solution was decanted leaving the product as a brilliant white powder (182.2 mg, 68%); IR: ν_{max} = 2095 (C-O str.), 2035 (C-O str.) 2001 (C-O str.) cm^{-1}.

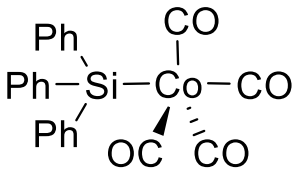

Cobalt(trichlorosilyl)(tetracarbonyl), $Co(CO)_4(Cl_3Si)$

This compound was synthesized using a modified preparation.[42] Cobalt carbonyl (202.7 mg, 0.593 mmol, 1 eq) was added to a glass vial and dissolved in 7 mL hexanes. The solution was added to a 100 mL Schlenk flask. Trichlorosilane (0.2 0mL, 1.979 mmol, 3.3 eq) was then syringed into the solution and left to react for 17 h at room temperature. The solution was dried *in vacuo* at room temperature. A cold finger was equipped to the Schlenk flask, and the product was sublimed using an oil bath at 40°C and static vacuum. The product was isolated from the cold finger as dense yellow crystals (238.4 mg, 66%); IR: ν_{max} = 2122 (C-O str.), 2069 (C-O str.) 2037 (C-O str.) cm^{-1}.

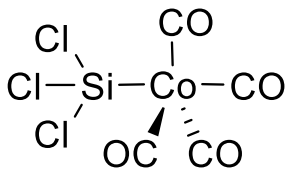

Cobalt(dichloromethylsilyl)(tetracarbonyl), $Co(CO)_4(Cl_2MeSi)$

Cobalt carbonyl (201.8 mg, 0.590 mmol, 1 eq) was added to a 100 mL Schlenk flask and chilled to -10°C in an ice bath. Dichloromethylsilane (5.5 mL, 52 mmol, excess) was syringed into the flask. After 1 h the ice bath was removed, and the solution was left to react for 1.5 h as it slowly warmed to room temperature. The solution was dried *in vacuo* and a cold finger was inserted into the flask. The product was sublimed using an oil bath at 50°C and static vacuum. The product was isolated as off-white crystals (244.0mg, 73%); IR: ν_{max} = 2113 (C-O str.), 2057 (C-O str.) 2022 (C-O str.) cm^{-1}.

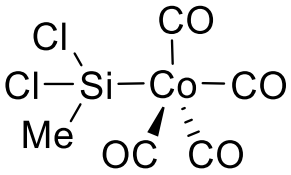

Cobalt(chlorodimethylsilyl)(tetracarbonyl), $Co(CO)_4(ClMe_2Si)$

Cobalt carbonyl (192.1 mg, 0.562 mmol, 1 eq) was added to a 100 mL Schlenk flask and chilled to -10°C in an ice bath. Chlorodimethylsilane (5.0 mL, 45 mmol, excess) was syringed into the flask. After 45 min the ice bath was removed, and the solution was left to react for 1 h as it slowly warmed to room temperature. The solution was dried *in vacuo* and a cold finger was inserted into the flask. The product was sublimed using an oil bath at 50°C and static vacuum. The product was isolated as dark brown crystals (60.0 mg, 40%); IR: ν_{max} = 2102 (C-O str.), 2042 (C-O str.) 2009 (C-O str.) cm^{-1}.

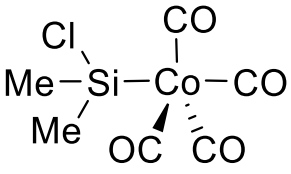

2.6.3 Charged Cobalt Carbonyl Synthesis

Dicobalt(hexacarbonyl)bis(benzylbis(diphenylphosphino)ethane)bis(hexafluorophosphate), $[Co_2(CO)_6(BPP)_2][(PF_6)_2]$

Cobalt carbonyl (71.1 mg, 0.208 mmol, 1 eq) was dissolved in 7 mL CH_2Cl_2 and filter pipetted into a 250 mL Schlenk flask. [BPP][PF_6] (130.7 mg, 0.206 mmol, 1 eq) was dissolved in 5 mL CH_2Cl_2 and pipetted into the cobalt solution. Bubbling was observed upon addition and the solution was left to react for 3 h. The solution was dried *in vacuo* with gentle heating. The solid was redissolved in minimal CH_2Cl_2 and filter pipetted into two glass vials. The solution was then layered in a 3:1 ratio of hexanes to CH_2Cl_2 and left to crystallize at room temperature for 1 day. The solution was then decanted, and the product was isolated as deep red crystals (71 mg, 44%); ESI-MS: $[Co_2(CO)_6(BPP)_2]^{2+}$ *m/z* 632, $[PF_6]^-$ *m/z* 145.

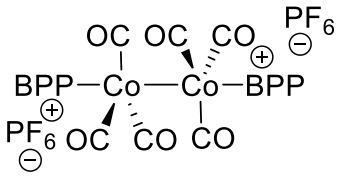

2.6.4 Charged Silyl Cobalt Precursor Syntheses

Cobalt(triscarbonyl)(triphenylsilyl)(benzylbis(diphenylphosphino)ethane)(hexafluorophosphate), [$Co(CO)_3(Ph_3Si)(BPP)][PF_6$]

Cobalt(tetracarbonyl)(triphenylsilyl) (30.0 mg, 0.070 mmol, 1 eq) was added to a 25 mL Schlenk flask and dissolved in 4 mL CH_2Cl_2. [BPP][PF_6] (47.2 mg, 0.074 mmol, 1.1 eq) was dissolved in 3 mL CH_2Cl_2 then syringed into the Schlenk flask. Bubbling was observed immediately upon addition and the solution was left to react for 1 day. Over the course of the reaction, the solution changed from black to deep orange. The solution was then transferred into two glass vials and the solutions were layered in a 3:1 ratio of hexanes to CH_2Cl_2 and left to crystallize for 1 day. The solutions were then decanted leaving a small amount of orange crystals (10.0 mg, 14%); ESI-MS: $[Ph_3SiCo(CO)_3(BPP)]^+$ *m/z* 891, $[PF_6]^-$ *m/z* 145.

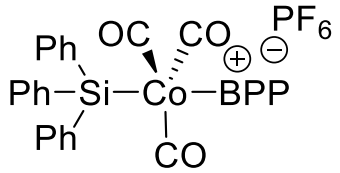

Cobalt(triscarbonyl)(tris(dimethylamino)silyl)(benzylbis(diphenylphosphino)ethane)(hexafluorophosphate), [$Co(CO)_3((Me_2N)_3Si)(BPP)][PF_6$]

[$Co_2(CO)_6(BPP)_2$][PF_6] (100.9 mg, 0.065 mmol, 1 eq) was added to a 100 mL Schlenk flask and suspended in 8 mL fluorobenzene and heated to 90°C. Tris(dimethylamino)silane (0.08 mL, 0.416 mmol, 6.4 eq) was syringed directly into the flask and the solution was allowed to react for 3.5 h.

The solution was concentrated *in vacuo* to roughly 2 mL and left to crystallize in the freezer overnight. The solution was then filter pipetted into another glass vial. The product was not purified further or isolated, but product formation was confirmed using MS. ESI-MS: $[(Me_2N)_3SiCo(CO)_3(BPP)]^+$ *m/z* 792, $[PF_6]^-$ *m/z* 145.

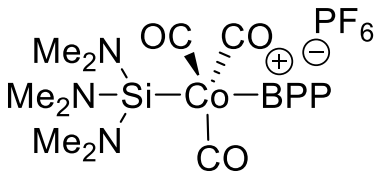

Cobalt(trichlorosilyl)(triscarbonyl)(triphenylphosphinomonosulfonate)bis(triphenylphosphine)iminium, $[Co(Cl_3Si)(CO)_3(TPPMS)][PPN]$

[TPPMS][PPN] (459 mg, 0.522 mmol, 0.8 eq) was added to a 50 mL Schlenk flask and dissolved in 5 mL CH_2Cl_2. Cobalt(tetracarbonyl)(trichlorosilyl) (202.1 mg, 0.662 mmol, 1 eq) was added to a glass vial and dissolved in 3 mL CH_2Cl_2 and pipetted into the TPPMS solution. Bubbles began to evolve immediately upon addition and the solution was left to react for 1 day. The solution changed colour from pale yellow to deep red over the course of the reaction. The solution was dried *in vacuo* and redissolved in minimal CH_2Cl_2 and transferred to a glass vial. Hexanes were added to solution dropwise until precipitate started to form. The solution was stored in the freezer for 1 day. The solution was then filter pipetted into another glass vial to remove the white precipitate produced as a decomposition by-product. The product was not purified further or isolated, but product formation was confirmed using MS. ESI-MS: $[Cl_3SiCo(CO)_3(TPPMS)]^-$ *m/z* 617, $[PPN]^+$ *m/z* 538.

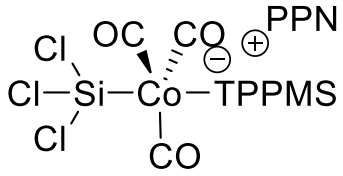

2.6.5 PSI-ESI-MS Experiments

This PSI-ESI-MS experiment was done qualitatively since the reactive charged cobalt precursor was not isolated from solution. 3 drops of the $[Co(Cl_3Si)(CO)_3(TPPMS)][PPN]$ solution in CH_2Cl_2 was diluted with 9 mL CH_2Cl_2 and syringed into a modified Schlenk flask.[16] The flask was attached to the ESI-MS and the flask was pressurized with argon. 0.1 mL ethanol was dissolved in 1 mL CH_2Cl_2 and syringed into the Schlenk flask to start the reaction. The sample was allowed to react for 3 h while data was being collected. After 3 h the experiment was complete, and the sample was discarded.

3 Understanding the Colour Change of Solutions of Cp_2TiCl upon addition of water

Portions of this chapter have been adapted from A. Rosales Martínez, L. Enríquez, M. Jaraíz, T. Thiessen, J. Sidhu, J.S. McIndoe, I. Rodríguez-García, "Understanding the color change of the solutions of Cp2TiCl upon addition of water", *Applied Organometallic Chemistry*, **2022**, Doi: 10.1002/aoc.6979. Tanner Thiessen completed the experimental preparation of the samples for MS analysis with the assistance of undergraduate mentee Jaspreet Sidhu. Analysis of results and writing was collaboratively done by Tanner Thiessen and Scott McIndoe. The computational work that made up the remainder of the paper was performed by the remaining authors.

3.1 Abstract

Reduction of red bis(cyclopendadienyl)titanium(IV) dichloride (Cp_2TiCl_2) with manganese dust in dry THF produces a green solution that turns deep blue upon the addition of traces of water. Mass spectrometric analysis has been performed to achieve a better understanding of the charged species that may be present after the interaction of water with reduced Cp_2TiCl_2. The deep blue solution provides a handy visual indicator for the qualitative determination of water in THF.

3.2 Introduction

Titanocene monochloride ($Cp_2Ti^{III}Cl$) is a single-electron transfer (SET) complex, recently proposed as a new green reagent, which can efficiently catalyze a wide range of synthetic processes with high diastereo- and regioselectivity.[45–54] This reagent can be easily prepared from commercial Cp_2TiCl_2 by using reductants such as elemental Mn or Zn.[55–57] Alternatively, electrochemical reduction,[58–60] organosilicon reducing agents,[61] and photoredox catalysis[62,63] can be used to obtain this SET complex from Cp_2TiCl_2. The nature of this SET complex in solution was reported by Skrydstrup et al.,[64] who indicated the existence of an equilibrium between dinuclear and mononuclear species (Pathway A, **Scheme 3.1**).

The initial reduction of Cp_2TiCl_2 to the titanocene(III) species can be easily visualized by a change in the colour of the solution when Mn or Zn is used as the reducing metal. When THF is the solvent, the initially orange-red solution of Cp_2TiCl_2 turns green after reduction indicating that the titanocene(III) species is formed.[55–57] However, when MeCN is the solvent, the solution finally turns deep blue as $[Cp_2Ti(NCMe)_2]^+$ is formed[65–67] (Pathway B, **Scheme 3.1**). In both cases,

oxidation of the titanium(III) species with molecular oxygen generates a yellow solution. This colour change has been used as an effective O_2 sensor in inert-atmosphere boxes, because if the blue solution of $[Cp_2Ti(NCMe)_2]^+$ is exposed to air, it rapidly discolours to bright yellow,[65–67] yielding $[Cp_2Ti(NCMe)(OMe)]^+$ (Pathway C, **Scheme 3.1**). This property makes the blue acetonitrile solution a useful visual indicator to detect the presence of trace oxygen.[67]

It has also been reported that in free-radical reactions mediated by this SET complex, water acts as a hydrogen atom donor.[68–70] However, the colour changes experienced by the THF solutions of this reagent in the presence of water have not been investigated. Therefore, a study of the molecular species responsible for the visual changes would be desirable, to gain a greater knowledge of the active species that can participate in the hydrogen atom transfer (HAT) processes. In addition, these insights could be useful for the development of a new colorimetric method to qualitatively determine the presence of water in THF.

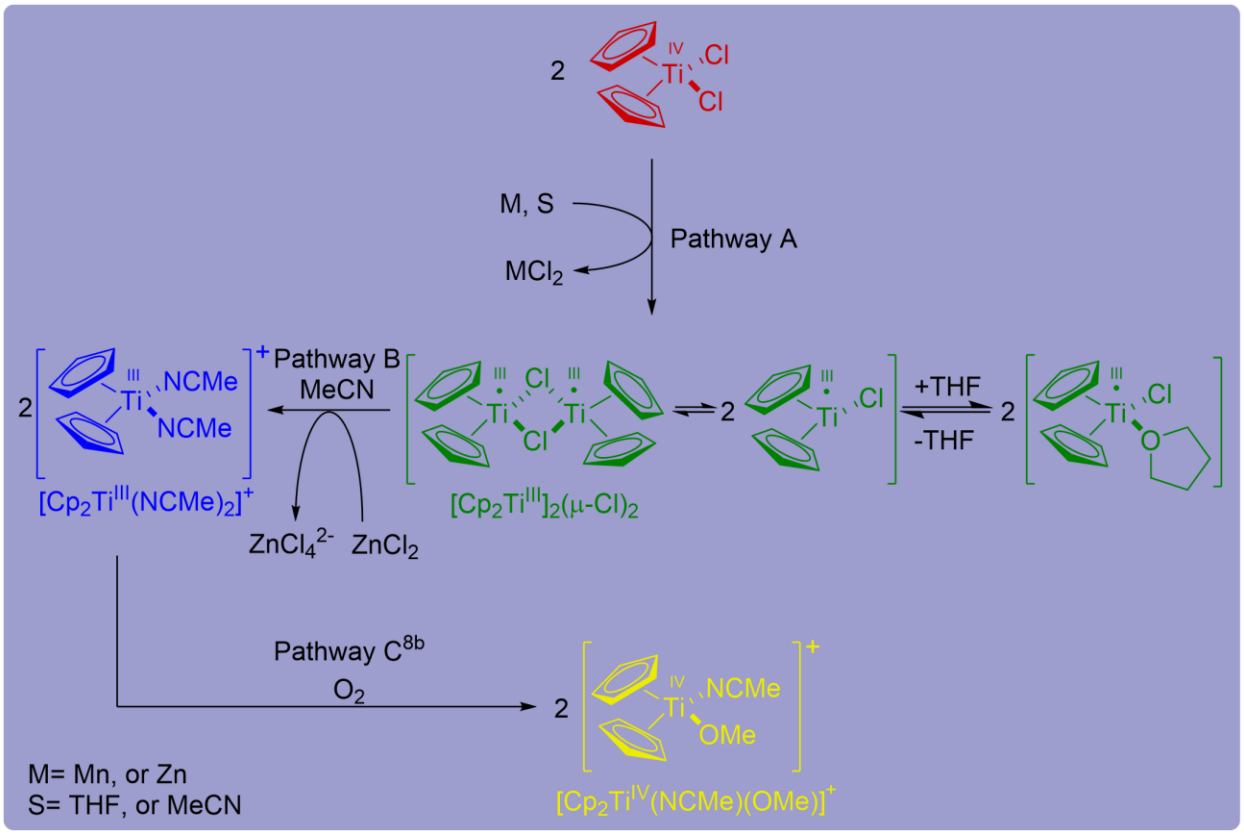

Scheme 3.1: Synthesis and subsequent oxidation of titanocene(III) species in MeCN and THF solution.

3.3 Results and Discussion

Experimentally, it is observed that when deoxygenated THF is added to a mixture of Cp_2TiCl_2 and Mn, the solution formed is initially red-orange (**Figure 3.1A**) then turns lime-green (**Figure 3.1B**) after 20 min. If the mixture is kept under an inert atmosphere, the colour remains unchanged (**Figure 3.1C**). If after stirring of this mixture for 30 min, water in THF is added, the lime-green solution turns into light green (**Figure 3.1D**) in just 2 min. Stirring of the reaction mixture under the same conditions slowly transforms the colour towards blue tonalities. In this way, 27 min after the addition of water, the solution takes a bluish-green colour (**Figure 3.1E**). Finally, the solution turns dark blue (**Figure 3.1F**).

Time (min)[a]

0	20	50	52	77	110
					
A	B	C	D	E	F

[a] Water was added after 50 min of the addition of THF to the Cp_2TiCl_2+Mn mixture.

Figure 3.1: Colour of a Ti(IV) solution in dry THF (A); colour of titanium(III) species solutions in dry THF (B, C); and colour change observed in the solution when water is added (D, E, F).

This striking color change from green to blue provides an immediate signal that new titanium-containing species are being formed. To corroborate the interaction of water with titanium(III) species in THF, quantum chemical calculations were carried out by our collaborators using density function theory (DFT). From their calculations they were able to theorize a mechanism of reaction for each of the colour changes observed; these findings are summarized in **Scheme 3.2**.

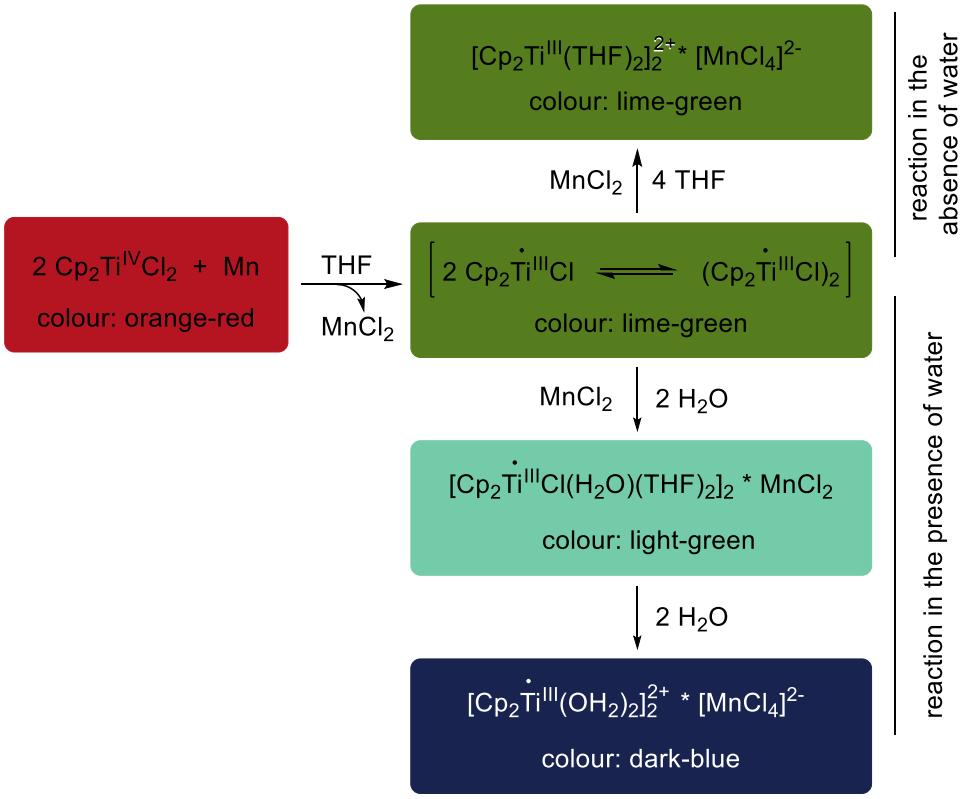

Scheme 3.2: Proposed mechanism and colour of the solution for the reduction of Cp_2TiCl_2.

To provide new insights, we turned to electrospray ionization mass spectrometry (ESI-MS). In the first stage of the reaction (orange/red solution, **Figure 3.1A**) no Ti-containing species were observed in the positive or negative ion mode mass spectra (as expected, as reduction has not yet occurred). After addition of Mn dust and conversion of the solution to lime-green (**Figure 3.1B**), we observed new charged species in both the positive and negative ion mode. The negative ion mode was dominated by aggregates of the form $[(MnCl_2)_nCl]^-$ (n = 1-3, **Figure 3.2**), at *m/z* 161.3, 287.1 and 412.9, with isotope patterns matching the calculated patterns of those species. Note that because dianionic species have a limited existence in the gas phase (there is no solvent around to stabilize them against loss of X^- or of an electron),[71] we would not expect to observe the dianionic $[MnCl_4]^{2-}$. The abundance of the aggregate ions suggests there is a substantial amount of neutral $MnCl_2$ present in solution, as expected for the reaction $2Cp_2TiCl_2 + Mn \rightarrow 2Cp_2TiCl + MnCl_2$.

An ion paired species was also observed with the overall composition $[MnCl_4Cp_2Ti]^-$ at *m/z* 375, which is probably best thought of as $[(MnCl_3)(Cp_2TiCl)]^-$ and that provides evidence both for the reduction of $Cp_2Ti^{IV}Cl_2$ to $Cp_2Ti^{III}Cl$ and the concomitant oxidation of Mn. Its abundance

suggests that there is a considerable amount of neutral $Cp_2Ti^{III}Cl$ present in solution. The *m/z* 374.8 ion decomposes in the gas phase under collision-induced dissociation (CID) to $[MnCl_3]^-$ at *m/z* 161.3, losing neutral $Cp_2Ti^{III}Cl$, and corroborating the assignment. The positive ion mode (**Figure 3.3**) was dominated by an ion at *m/z* 250.1, which can be assigned to $[Cp_2Ti^{III}(THF)]^+$. This ion likely arises from loss of halide from $Cp_2Ti^{III}Cl$, a well-known ionization pathway for metal complexes in polar solvents in ESI-MS.[72] It decomposes when fragmented by CID to $[Cp_2Ti]^+$ at *m/z* 178, i.e. loss of neutral THF.

Further analysis of solutions after H_2O addition did not reveal the presence of new charged Ti-containing species in either ion mode, despite the evident colour changes. However, note that both $Cp_2Ti^{III}Cl$ and the dimer $[Cp_2Ti^{III}(OH_2)_2]_2^{2+}$ are both likely to provide the same ion in ESI-MS analysis in THF solution, namely $[Cp_2Ti^{III}(THF)]^+$, because the former can only acquire a charge via chloride ion loss, and the water ligands are unlikely to be tenacious enough binders to survive the desolvation process. The appearance of THF as a ligand arises because of its large excess, present as it is as a solvent.

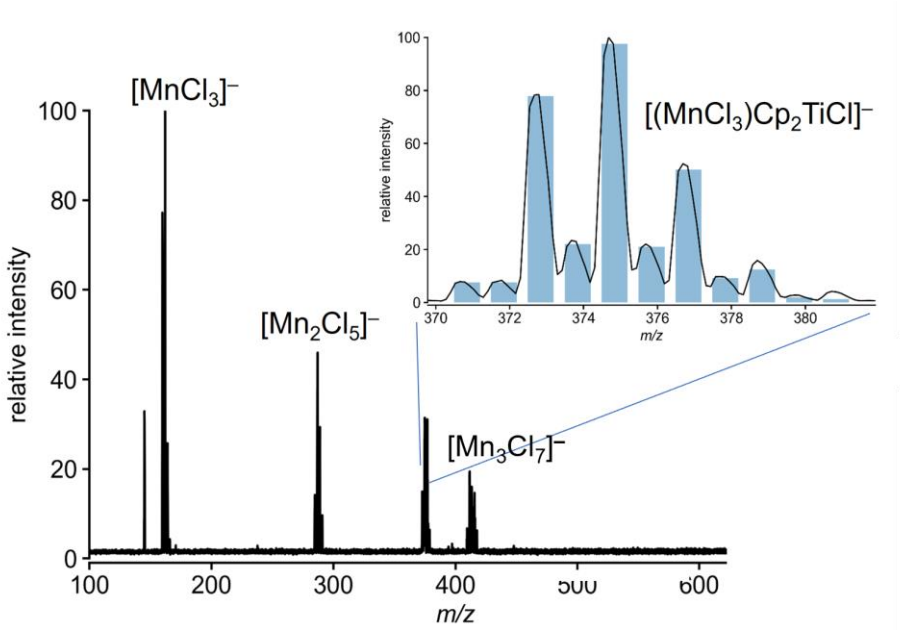

Figure 3.2: Negative ion mode full spectrum of the anhydrous THF solution generated by reduction of Cp_2TiCl_2 with manganese dust, inset shows experimental and calculated isotope patterns for $[(MnCl_3)Cp_2TiCl]^-$

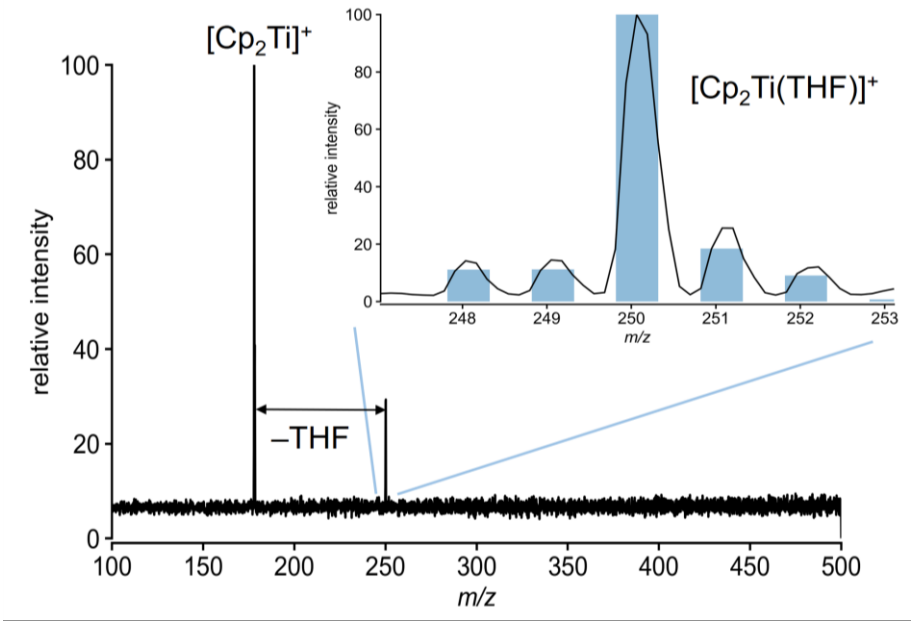

Figure 3.3: Positive ion mode product ion MS/MS spectrum for $[Cp_2Ti(THF)]^+$ in the anhydrous THF solution generated by reduction of Cp_2TiCl_2 with manganese dust, inset shows experimental and calculated isotope patterns for the precursor ion.

This preliminary result provides solid experimental evidence of the effect of water on the change of colour suffered by the initially lime-green titanocene(III) solution in THF. In addition, the change of colour is a handy colorimetric visual indicator that allows the detection of water in THF. For this purpose, the colour change of different solutions of titanocene(III) in THF has been monitored (**Table 3.1**). The role played by water was studied performing a series of five experiments with decreasing amounts of this reagent (entries 1-5, **Table 3.1**). In all cases, the initially green solution of Cp_2TiCl turned dark blue. On the other hand, under a strict absence of water, no dark blue species could be detected even after prolonged reaction times (entry 6, **Table 3.1**). These results confirm that the colour of the titanium species in THF can be used as a colorimetric indicator for the qualitatively determination of the presence of water in THF. The described procedure permits the determination of the presence of water in THF in concentrations as low as 0.07%.

Table 3.1: Time evolution of the colour of the reaction

Entry	Cp_2TiCl_2 (mmol)	Mn (mmol)	Solvent (THF[a] (mL)/H_2O[b] (µL)	Lime-green colour (min[d])	Dark blue colour (min[d])
1	0.25	0.9	15 / 152	30	60
2	0.25	0.9	15 / 75	30	60
3	0.25	0.9	15 / 38	30	60
4	0.25	0.9	15 / 19	30	60
5	0.25	0.9	15 / 9	30	60
6[c]	0.25	0.9	15 / 0	30	-

[a] THF was dried and distilled from Na/benzophenone under argon and was deoxygenated prior to use.

[b] Water was deoxygenated prior to use.

[c] Continuous green solution after stirring 5 h.

[d] Time measured from the start of the reaction.

3.4 Conclusion

In summary, an inexpensive, safe, simple and green method for the qualitative determination of water in THF based on colour change of green titanocene species to blue solution, is described. A detailed experimental study of the effect of water concentration on colour change is reported. In addition, ESI-MS confirmed the presence of $Cp_2Ti^{III}Cl$ through the observation of $[(Cp_2TiCl)(MnCl_3)]^-$ in the negative ion mode, and cationic Ti^{III} species through the observation of $[Cp_2Ti(THF)]^+$ in the positive ion mode.

3.5 Materials and Methods

All reagents and solvents were purchased from Sigma-Aldrich and used as received unless noted below. 4 Å molecular sieves were dried by heating them for 2 h via flame, under vacuum. HPLC-grade THF was distilled from Na/benzophenone under a nitrogen atmosphere onto dried 4 Å molecular sieves. Due to the air-sensitivity of the reaction, THF and deionized water were deoxygenated prior to use by bubbling a stream of nitrogen through them for 5 min.

The compounds used in these experiments were air and moisture sensitive so special considerations were made when handling these compounds for MS acquisition outside of the glovebox.[41] All mass spectra were collected by a Waters Acquity Triple Quadrupole Mass spectrometer equipped with a Z-Spray pneumatically assisted electrospray ionization source in the positive or negative ion mode. Instrument source parameters were as follows: capillary voltage was held at 3 kV, cone voltage at 15 V. The following settings were used for desolvation

conditions: desolvation gas flow rate, 100 L/h; cone gas flow rate, 100 L/h; source temperature, 75°C; desolvation temperature, 150°C.

The reaction was carried out on a Schlenk line using standard Schlenk techniques. To prepare a MS sample, a glass syringe was purged with nitrogen three times before being used to transfer a sample of the reaction into a 50 mL Schlenk flask, which was then transferred into the glovebox. The solution was gravity filtered into a glass vial. 1 mL of this solution was diluted with 4 mL of THF before loading into a 1 mL plastic syringe. The syringe had a needle attached to the end and was stabbed into a rubber stopper to decrease atmospheric contamination while handling outside the glovebox. The syringe and stopper were transferred out of the glovebox and the syringe was attached to the MS via PEEK tubing. Each MS sample was prepared in this way. This preparation allowed for MS samples to be prepared without the unwanted introduction of either air or water.

Cp_2TiCl_2 (125 mg, 0.502 mmol, 1 eq) and Manganese dust (99 mg, 1.802 mmol, excess) was added to a 100 mL Schlenk flask. 27 mL of THF was syringed into the flask. The solution was red, and a MS sample was obtained. The Schlenk flask was heated to 25°C. After 1.5 h the solution had turned green, and a MS sample was obtained. 1mL of deionized water was added to 50 mL of THF. 15 mL of this solution was injected into the Schlenk flask over 2 min. This caused immediate conversion from green to blue. After 2 h, the solution was still blue, and a MS sample was obtained. Each sample would turn orange if at any point they came in contact with oxygen.

4 Summary and Outlook

Air– and moisture–sensitive compounds can be difficult to monitor and handle because sample introduction typically causes small amounts of air and moisture to enter the sample and cause degradation. ESI-MS and PSI-ESI-MS were demonstrated to be efficient techniques at limiting sample exposure to air and moisture when handled correctly. This efficacy was particularly evident when using ESI-MS to study the reaction of Cp_2TiCl_2 in THF with deoxygenated water. The solution undergoes colour change from red to green when it forms its reactive state and turns blue when deoxygenated water is manually introduced. If at any point the solution came into contact with air, the whole sample would degrade to a yellow colour almost immediately. Real time experimental data was acquired using PSI-ESI-MS for the reaction between charged ALD precursors and EtOH. These reactions occur in micro molar concentrations so this reaction would degrade immediately if air and moisture were able to enter the reaction vessel.

This thesis established pathways to the synthesis of compounds of the type $X_3SiCo(CO)_3L$ (where X = halide, OR, or NR_2 and L = charge-tagged ligand). Preliminary reactivity studies between the model compounds and alcohols showed that the real-time analysis of these compounds is feasible. Preliminary testing showed interaction between silsesquioxane and $[Cl_3SiCo(CO)_3(TPPMS)][PPN]$ but this interaction could not be fully explained. Interaction between the charged tag and silsesquioxane was ruled out so this interaction must involve the silsesquioxane and the precursor in some way.

Further purification and identification of charged ALD precursors should be conducted first. Afterwards reaction monitoring experiments can continue with silsesquioxane to try and identify what issues may be occurring. If silsesquioxane is ultimately found to be a poor model compound to use for these studies, then various silanols (including disilanols and trisilanols) should be explored as substitutes.

In tandem with this work, Sofia Donnecke of the McIndoe and Paci groups has performed computational analysis of the reaction of $X_3SiCo(CO)_4$ compounds with surfaces, and the results from her work will be combined with the results obtained here to provide new insights into this hitherto unexplored chemistry.

References

(1) Gross, J. H. *Mass Spectrometry*; Springer International Publishing: Cham, 2017. https://doi.org/10.1007/978-3-319-54398-7.

(2) de Hoffmann, E. *Mass Spectrometry: Principles and Applications*; John Wiley & Sons, Incorporated: Newark, UNITED STATES, 2007.

(3) Maux, D.; Enjalbal, C.; Martinez, J.; Aubagnac, J.-L.; Combarieu, R. Static Secondary Ion Mass Spectrometry to Monitor Solid-Phase Peptide Synthesis. *J. Am. Soc. Mass Spectrom.* **2001**, *12* (10), 1099–1105. https://doi.org/10.1016/S1044-0305(01)00296-3.

(4) Petrie, S.; Bohme, D. K. Ions in Space. *Mass Spectrom. Rev.* **2007**, *26* (2), 258–280. https://doi.org/10.1002/mas.20114.

(5) Dole, M.; Mack, L. L.; Hines, R. L.; Mobley, R. C.; Ferguson, L. D.; Alice, M. B. Molecular Beams of Macroions. *J. Chem. Phys.* **1968**, *49* (5), 2240–2249. https://doi.org/10.1063/1.1670391.

(6) Fenn, J. B.; Mann, M.; Meng, C. K.; Wong, S. F.; Whitehouse, C. M. Electrospray Ionization for Mass Spectrometry of Large Biomolecules. *Science* **1989**, *246* (4926), 64–71. https://doi.org/10.1126/science.2675315.

(7) Bruins, A. P. Mechanistic Aspects of Electrospray Ionization. *J. Chromatogr. A* **1998**, *794* (1), 345–357. https://doi.org/10.1016/S0021-9673(97)01110-2.

(8) Ho, C.; Lam, C.; Chan, M.; Cheung, R.; Law, L.; Lit, L.; Ng, K.; Suen, M.; Tai, H. Electrospray Ionisation Mass Spectrometry: Principles and Clinical Applications. *Clin. Biochem. Rev.* **2003**, *24* (1), 3–12.

(9) *Quadrupole Ion Trap Mass Spectrometry*, 1st ed.; John Wiley & Sons, Ltd, 2005. https://doi.org/10.1002/0471717983.

(10) Evans, W. J.; Johnston, M. A.; Fujimoto, C. H.; Greaves, J. Utility of Electrospray Mass Spectrometry for the Characterization of Air-Sensitive Organolanthanides and Related Species [1]. *Organometallics* **2000**, *19* (21), 4258–4265. https://doi.org/10.1021/om000178u.

(11) Vikse, K. L.; Woods, M. P.; McIndoe, J. S. Pressurized Sample Infusion for the Continuous Analysis of Air- And Moisture-Sensitive Reactions Using Electrospray Ionization Mass Spectrometry. *Organometallics* **2010**, *29* (23), 6615–6618. https://doi.org/10.1021/om1008082.

(12) Lubben, A. T.; McIndoe, J. S.; Weller, A. S. Coupling an Electrospray Ionization Mass Spectrometer with a Glovebox: A Straightforward, Powerful, and Convenient Combination for Analysis of Air-Sensitive Organometallics. *Organometallics* **2008**, *27* (13), 3303–3306. https://doi.org/10.1021/om800164e.

(13) Williams, D. B. G.; Lawton, M. Drying of Organic Solvents: Quantitative Evaluation of the Efficiency of Several Desiccants. *J. Org. Chem.* **2010**, *75* (24), 8351–8354. https://doi.org/10.1021/jo101589h.

(14) Joshi, A.; Donnecke, S.; Granot, O.; Shin, D.; Collins, S.; Paci, I.; Scott McIndoe, J. Reactive Metallocene Cations as Sensitive Indicators of Gas-Phase Oxygen and Water. *Dalton Trans.* **2020**, *49* (21), 7028–7036. https://doi.org/10.1039/D0DT00798F.

(15) Santos, L. S.; Rosso, G. B.; Pilli, R. A.; Eberlin, M. N. The Mechanism of the Stille Reaction Investigated by Electrospray Ionization Mass Spectrometry. *J. Org. Chem.* **2007**, *72* (15), 5809–5812. https://doi.org/10.1021/jo062512n.

(16) Thomas, G. T.; MacGillivray, L.; Dean, N. L.; Stoddard, R. L.; Yunker, L. P. E.; McIndoe, J. S. Confounding Contaminants in Mass Spectrometric Reaction Monitoring. *Int. J. Mass Spectrom.* **2019**, *441*, 14–18. https://doi.org/10.1016/j.ijms.2019.04.001.

(17) Hesketh, A. V.; Nowicki, S.; Baxter, K.; Stoddard, R. L.; McIndoe, J. S. Simplified Real-Time Mass Spectrometric Analysis of Reactions. *Organometallics* **2015**, *34* (15), 3816–3819. https://doi.org/10.1021/acs.organomet.5b00460.

(18) Joshi, A.; Zijlstra, H. S.; Collins, S.; McIndoe, J. S. Catalyst Deactivation Processes during 1-Hexene Polymerization. *ACS Catal.* **2020**, *10* (13), 7195–7206. https://doi.org/10.1021/acscatal.0c01607.

(19) Zijlstra, H. S.; Joshi, A.; Linnolahti, M.; Collins, S.; McIndoe, J. S. Modifying Methylalumoxane *via* Alkyl Exchange. *Dalton Trans.* **2018**, *47* (48), 17291–17298. https://doi.org/10.1039/C8DT04242J.

(20) Kol'tsov, S. Interaction of Trichlorosilane with Silica Gel. *J. Appl. Chem. USSR* **1965**, *38*, 1352–1384.

(21) Cremers, V.; Puurunen, R. L.; Dendooven, J. Conformality in Atomic Layer Deposition: Current Status Overview of Analysis and Modelling. *Appl. Phys. Rev.* **2019**, *6* (2), 021302. https://doi.org/10.1063/1.5060967.

(22) Johnson, R. W.; Hultqvist, A.; Bent, S. F. A Brief Review of Atomic Layer Deposition: From Fundamentals to Applications. *Mater. Today* **2014**, *17* (5), 236–246. https://doi.org/10.1016/j.mattod.2014.04.026.

(23) Leskelä, M.; Ritala, M. Atomic Layer Deposition (ALD): From Precursors to Thin Film Structures. *Thin Solid Films* **2002**, *409* (1), 138–146. https://doi.org/10.1016/S0040-6090(02)00117-7.

(24) Knez, M.; Nielsch, K.; Niinistö, L. Synthesis and Surface Engineering of Complex Nanostructures by Atomic Layer Deposition. *Adv. Mater.* **2007**, *19* (21), 3425–3438. https://doi.org/10.1002/adma.200700079.

(25) Kwon, J.; Saly, M.; Kanjolia, R. K.; Chabal, Y. J. Surface Reactions of M2-H2-(TBu-Acetylene)Dicobalthexacarbonyl with Oxidized and H-Terminated Si(111) Surfaces. *Chem. Mater.* **2011**, *23* (8), 2068–2074. https://doi.org/10.1021/cm103028x.

(26) Johnson, A. L.; Parish, J. D. Recent Developments in Molecular Precursors for Atomic Layer Deposition. **2018**, 1–53. https://doi.org/10.1039/9781788010672-00001.

(27) Potts, S. E.; Kessels, W. M. M. Energy-Enhanced Atomic Layer Deposition for More Process and Precursor Versatility. *Coord. Chem. Rev.* **2013**, *257* (23–24), 3254–3270. https://doi.org/10.1016/j.ccr.2013.06.015.

(28) Oviroh, P. O.; Akbarzadeh, R.; Pan, D.; Coetzee, R. A. M.; Jen, T.-C. New Development of Atomic Layer Deposition: Processes, Methods and Applications. *Sci. Technol. Adv. Mater.* **2019**, *20* (1), 465–496. https://doi.org/10.1080/14686996.2019.1599694.

(29) George, S. M. Atomic Layer Deposition: An Overview. *Chem. Rev.* **2010**, *110* (1), 111–131. https://doi.org/10.1021/cr900056b.

(30) Bakke, J. R.; Pickrahn, K. L.; Brennan, T. P.; Bent, S. F. Nanoengineering and Interfacial Engineering of Photovoltaics by Atomic Layer Deposition. *Nanoscale* **2011**, *3* (9), 3482–3508. https://doi.org/10.1039/C1NR10349K.

(31) Dwivedi, V. H.; Hasegawa, M.; Adomaitis, R. A.; Salami, H.; Uy, A.; Grob, C.; Vadapalli, A. Application and Development of Atomic Layer Deposition Techniques to Improve Thermo-Optical Coatings for Spacecraft Thermal Control and Advanced Optical Instruments. 9.

(32) Berger, L. I. Introduction to Semiconductor Physics. In *Semiconductor Materials*; CRC Press, 1997; pp 15–35.

(33) *Atomic Layer Deposition for Semiconductors*; Hwang, C. S., Ed.; Springer US: Boston, MA, 2014. https://doi.org/10.1007/978-1-4614-8054-9.

(34) Kwon, J.; Saly, M.; Halls, M. D.; Kanjolia, R. K.; Chabal, Y. J. Substrate Selectivity of (TBu-Allyl)Co(CO)3 during Thermal Atomic Layer Deposition of Cobalt. *Chem. Mater.* **2012**, *24* (6), 1025–1030. https://doi.org/10.1021/cm2029189.

(35) Berry, R. S. Correlation of Rates of Intramolecular Tunneling Processes, with Application to Some Group V Compounds. 6.

(36) Joyce, B. A.; Bradley, R. R. A Study of Nucleation in Chemically Grown Epitaxial Silicon Films Using Molecular Beam Techniques I.—Experimental Methods. *Philos. Mag.* **1966**, *14* (128), 289–299. https://doi.org/10.1080/14786436608219012.

(37) Cordes, D. B.; Lickiss, P. D.; Rataboul, F. Recent Developments in the Chemistry of Cubic Polyhedral Oligosilsesquioxanes. *Chem. Rev.* **2010**, *110* (4), 2081–2173. https://doi.org/10.1021/cr900201r.

(38) Chalk, A. J.; Harrod, J. F. Reactions between Dicobalt Octacarbonyl and Silicon Hydrides. *J. Am. Chem. Soc.* **1965**, *87* (5), 1133–1135. https://doi.org/10.1021/ja01083a035.

(39) Chisholm, D. M.; Oliver, A. G.; McIndoe, J. S. Mono-Alkylated Bisphosphines as Dopants for ESI-MS Analysis of Catalytic Reactions. *Dalton Trans.* **2009**, *39* (2), 364–373. https://doi.org/10.1039/B913225B.

(40) Forbus, P.; Smith, G.; Brown, L. EVIDENCE FOR A RADICAL CHAIN PATHWAY FOR SUBSTITUTION OF COZ(CO)8. 4.

(41) Joshi, A.; Killeen, C.; Thiessen, T.; Zijlstra, H. S.; McIndoe, J. S. Handling Considerations for the Mass Spectrometry of Reactive Organometallic Compounds. *J. Mass Spectrom.* **2022**, *57* (3), e4807. https://doi.org/10.1002/jms.4807.

(42) Novak, I.; Huang, W.; Luo, L.; Huang, H. H.; Ang, H. G.; Zybill, C. E. UPS Study of Compounds with Metal−Silicon Bonds: $M(CO)_n SiCl_3$ (M = Co, Mn; *n* = 4, 5) and $Fe(CO)_4(SiCl_3)_2$. *Organometallics* **1997**, *16* (8), 1567–1572. https://doi.org/10.1021/om960692t.

(43) Vikse, K. L.; Henderson, M. A.; Oliver, A. G.; McIndoe, J. S. Direct Observation of Key Intermediates by Negative-Ion Electrospray Ionisation Mass Spectrometry in Palladium-Catalysed Cross-Coupling. *Chem. Commun.* **2010**, *46* (39), 7412. https://doi.org/10.1039/c0cc02773a.

(44) McIndoe, J. S.; Nicholson, B. K. Facile Cleavage of Si–Si or Si–Ge Bonds in the Reactions of Disilanes or Germylsilanes with Cobalt Carbonyl. *J. Organomet. Chem.* **1999**, *577* (2), 181–188. https://doi.org/10.1016/S0022-328X(98)01016-X.

(45) Castro Rodríguez, M.; Rodríguez García, I.; Rodríguez Maecker, R. N.; Pozo Morales, L.; Oltra, J. E.; Rosales Martínez, A. Cp2TiCl: An Ideal Reagent for Green Chemistry? *Org. Process Res. Dev.* **2017**, *21* (7), 911–923. https://doi.org/10.1021/acs.oprd.7b00098.

(46) Martínez, A. R.; Rodríguez, M. C.; Rodríguez-García, I.; Morales, L. P.; Maecker, R. N. R. Titanocene Dichloride: A New Green Reagent in Organic Chemistry. *Chin. J. Catal.* **2017**, *38* (10), 1659–1663. https://doi.org/10.1016/S1872-2067(17)62894-8.

(47) Padial, N. M.; Roldan-Molina, E.; Rosales, A.; Álvarez-Corral, M.; Rodríguez-García, I.; Muñoz-Dorado, M.; Oltra, J. E. Chapter 2 - Stereoselective Synthesis of Natural Products Promoted by Titanocene(III). In *Studies in Natural Products Chemistry*; Atta-ur-Rahman, Ed.; Elsevier, 2018; Vol. 55, pp 31–71. https://doi.org/10.1016/B978-0-444-64068-0.00002-4.

(48) Botubol-Ares, J. M.; Durán-Peña, M. J.; Hanson, J. R.; Hernández-Galán, R.; Collado, I. G. Cp2Ti(III)Cl and Analogues as Sustainable Templates in Organic Synthesis. *Synthesis* **2018**, *50* (11), 2163–2180. https://doi.org/10.1055/s-0036-1591986.

(49) Gansäuer, A. From Enantioselective to Regiodivergent Epoxide Opening and Radical Arylation – Useful or Just Interesting? *Synlett* **2021**, *32* (05), 447–456. https://doi.org/10.1055/s-0040-1706407.

(50) Gansäuer, A.; Justicia, J.; Fan, C.-A.; Worgull, D.; Piestert, F. Reductive C–C Bond Formation after Epoxide Opening via Electron Transfer. In *Metal Catalyzed Reductive C–C Bond Formation: A Departure from Preformed Organometallic Reagents*; Krische, M. J., Ed.; Topics in Current Chemistry; Springer: Berlin, Heidelberg, 2007; pp 25–52. https://doi.org/10.1007/128_2007_130.

(51) Rosales, A.; Rodríguez-García, I.; Muñoz-Bascón, J.; Roldan-Molina, E.; Padial, N. M.; Morales, L. P.; García-Ocaña, M.; Oltra, J. E. The Nugent Reagent: A Formidable Tool in Contemporary Radical and Organometallic Chemistry. *Eur. J. Org. Chem.* **2015**, *2015* (21), 4567–4591. https://doi.org/10.1002/ejoc.201500292.

(52) Rosales, A.; Rodríguez-García, I.; Muñoz-Bascón, J.; Roldan-Molina, E.; Padial, N. M.; Morales, L. P.; García-Ocaña, M.; Oltra, J. E. The Nugent–RajanBabu Reagent: A Formidable Tool in Contemporary Radical and Organometallic Chemistry. *Eur. J. Org. Chem.* **2015**, *2015* (21), 4592–4592. https://doi.org/10.1002/ejoc.201500761.

(53) Martínez, A. R.; Morales, L. P.; Ojeda, E. D.; Rodríguez, M. C.; Rodríguez-García, I. The Proven Versatility of Cp2TiCl. *J. Org. Chem.* **2021**, *86* (2), 1311–1329. https://doi.org/10.1021/acs.joc.0c01233.

(54) Barrero, A. F.; Quílez del Moral, J. F.; Sánchez, E. M.; Arteaga, J. F. Titanocene-Mediated Radical Cyclization: An Emergent Method Towards the Synthesis of Natural Products. *Eur. J. Org. Chem.* **2006**, *2006* (7), 1627–1641. https://doi.org/10.1002/ejoc.200500849.

(55) RajanBabu, T. V.; Nugent, W. A.; Beattie, M. S. Free Radical-Mediated Reduction and Deoxygenation of Epoxides. *J. Am. Chem. Soc.* **1990**, *112* (17), 6408–6409. https://doi.org/10.1021/ja00173a045.

(56) RajanBabu, T. V.; Nugent, W. A. Intermolecular Addition of Epoxides to Activated Olefins: A New Reaction. *J. Am. Chem. Soc.* **1989**, *111* (12), 4525–4527. https://doi.org/10.1021/ja00194a073.

(57) Nugent, W. A.; RajanBabu, T. V. Transition-Metal-Centered Radicals in Organic Synthesis. Titanium(III)-Induced Cyclization of Epoxy Olefins. *J. Am. Chem. Soc.* **1988**, *110* (25), 8561–8562. https://doi.org/10.1021/ja00233a051.

(58) Liedtke, T.; Hilche, T.; Klare, S.; Gansäuer, A. Condition Screening for Sustainable Catalysis in Single-Electron Steps by Cyclic Voltammetry: Additives and Solvents. *ChemSusChem* **2019**, *12* (13), 3166–3171. https://doi.org/10.1002/cssc.201900344.

(59) Samuel, E.; Vedel, J. Electrochemical and Chemical Reduction of Titanocene Dihalides - an ESR Study. *Organometallics* **1989**, *8* (1), 237–241. https://doi.org/10.1021/om00103a031.

(60) Enemaerke, R. J.; Larsen, J.; Skrydstrup, T.; Daasbjerg, K. Mechanistic Investigation of the Electrochemical Reduction of Cp2TiX2. *Organometallics* **2004**, *23* (8), 1866–1874. https://doi.org/10.1021/om034360h.

(61) Saito, T.; Nishiyama, H.; Tanahashi, H.; Kawakita, K.; Tsurugi, H.; Mashima, K. 1,4-Bis(Trimethylsilyl)-1,4-Diaza-2,5-Cyclohexadienes as Strong Salt-Free Reductants for Generating Low-Valent Early Transition Metals with Electron-Donating Ligands. *J. Am. Chem. Soc.* **2014**, *136* (13), 5161–5170. https://doi.org/10.1021/ja501313s.

(62) Zhang, Z.; Hilche, T.; Slak, D.; Rietdijk, N. R.; Oloyede, U. N.; Flowers II, R. A.; Gansäuer, A. Titanocenes as Photoredox Catalysts Using Green-Light Irradiation. *Angew. Chem. Int. Ed.* **2020**, *59* (24), 9355–9359. https://doi.org/10.1002/anie.202001508.

(63) Zhang, Z.; Richrath, R. B.; Gansäuer, A. Merging Catalysis in Single Electron Steps with Photoredox Catalysis—Efficient and Sustainable Radical Chemistry. *ACS Catal.* **2019**, *9* (4), 3208–3212. https://doi.org/10.1021/acscatal.9b00787.

(64) Enemaerke, R. J.; Hjollund, G. H.; Daasbjerg, K.; Skrydstrup, T. Is the Trinuclear Complex the True Reducing Species in the Cp2TiCl2/Mn- and Cp2TiCl2/Zn-Promoted Pinacol Coupling? - ScienceDirect. *Comptes Rendus Académie Sci. - Ser. IIC - Chem.* **2001**, *4*, 435–438. https://doi.org/10.1016/s1387-1609(01)01259-2.

(65) Seewald, P. A.; White, G. S.; Stephan, D. W. Cationic Complexes of Titanium(III); Phosphine Substitution Reactions. *Can. J. Chem.* **1988**, *66* (5), 1147–1152. https://doi.org/10.1139/v88-188.

(66) Yeung, D.; Penafiel, J.; Zijlstra, H. S.; McIndoe, J. S. Oxidation of Titanocene(III): The Deceptive Simplicity of a Color Change. *Inorg. Chem.* **2018**, *57* (1), 457–461. https://doi.org/10.1021/acs.inorgchem.7b02705.

(67) Burgmayer, S. J. N. Use of a Titanium Metallocene as a Colorimetric Indicator for Learning Inert Atmosphere Techniques. *J. Chem. Educ.* **1998**, *75* (4), 460. https://doi.org/10.1021/ed075p460.

(68) Cuerva, J. M.; Campaña, A. G.; Justicia, J.; Rosales, A.; Oller-López, J. L.; Robles, R.; Cárdenas, D. J.; Buñuel, E.; Oltra, J. E. Water: The Ideal Hydrogen-Atom Source in Free-Radical Chemistry Mediated by TiIII and Other Single-Electron-Transfer Metals? *Angew. Chem. Int. Ed.* **2006**, *45* (33), 5522–5526. https://doi.org/10.1002/anie.200600831.

(69) Paradas, M.; Campaña, A. G.; Jiménez, T.; Robles, R.; Oltra, J. E.; Buñuel, E.; Justicia, J.; Cárdenas, D. J.; Cuerva, J. M. Understanding the Exceptional Hydrogen-Atom Donor Characteristics of Water in TiIII-Mediated Free-Radical Chemistry. *J. Am. Chem. Soc.* **2010**, *132* (36), 12748–12756. https://doi.org/10.1021/ja105670h.

(70) Gansäuer, A.; Behlendorf, M.; Cangönül, A.; Kube, C.; Cuerva, J. M.; Friedrich, J.; van Gastel, M. H2O Activation for Hydrogen-Atom Transfer: Correct Structures and Revised Mechanisms. *Angew. Chem. Int. Ed.* **2012**, *51* (13), 3266–3270. https://doi.org/10.1002/anie.201107556.

(71) Butcher, C. P. G.; Johnson, B. F. G.; McIndoe, J. S.; Yang, X.; Wang, X.-B.; Wang, L.-S. Collision-Induced Dissociation and Photodetachment of Singly and Doubly Charged Anionic Polynuclear Transition Metal Carbonyl Clusters: Ru3Co(CO)13−, Ru6C(CO)162−, and Ru6(CO)182−. *J. Chem. Phys.* **2002**, *116* (15), 6560–6566. https://doi.org/10.1063/1.1462579.

(72) McIndoe, J. S.; Vikse, K. L. Assigning the ESI Mass Spectra of Organometallic and Coordination Compounds. *J. Mass Spectrom.* **2019**, *54* (5), 466–479. https://doi.org/10.1002/jms.4359.

Appendices

Appendix A – IR Spectra

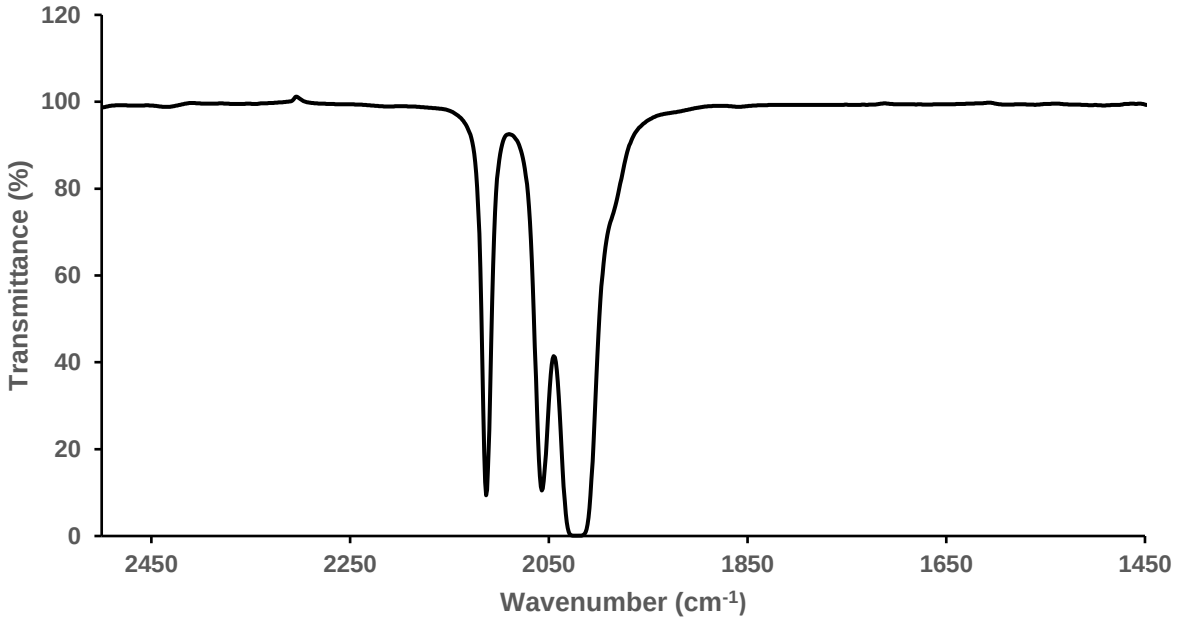

Figure A.1: Solution cell IR spectrum displaying the carbonyl stretching region of $Cl_2MeSiCo(CO)_4$ in CH_2Cl_2.

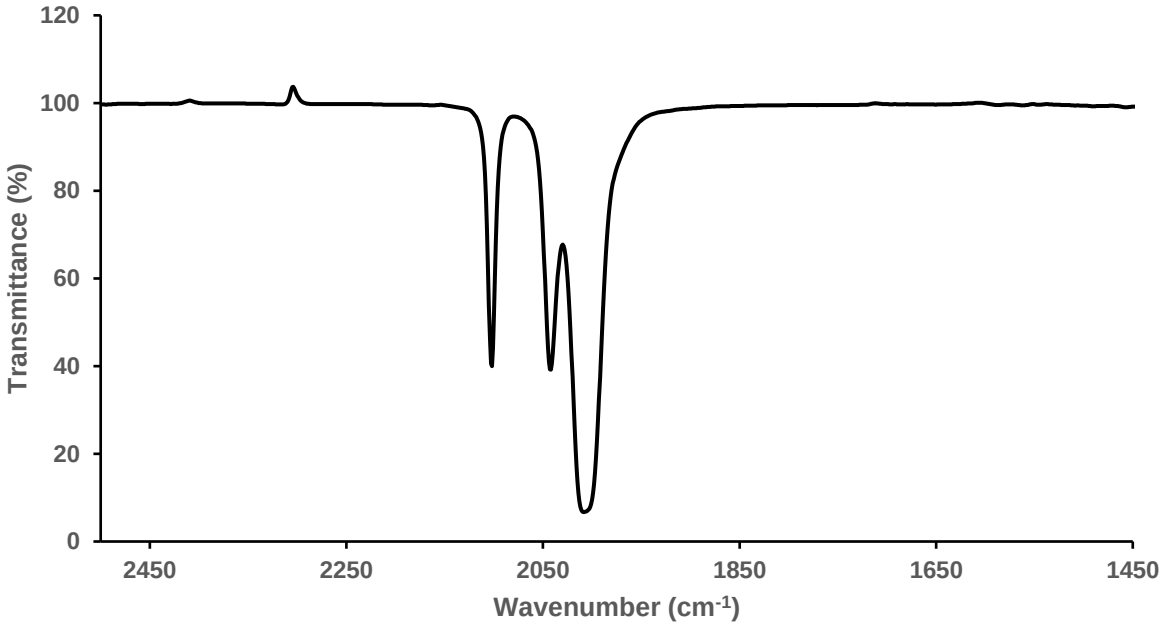

Figure A.2: Solution cell IR spectrum displaying the carbonyl stretching region of $ClMe_2SiCo(CO)_4$ in CH_2Cl_2.

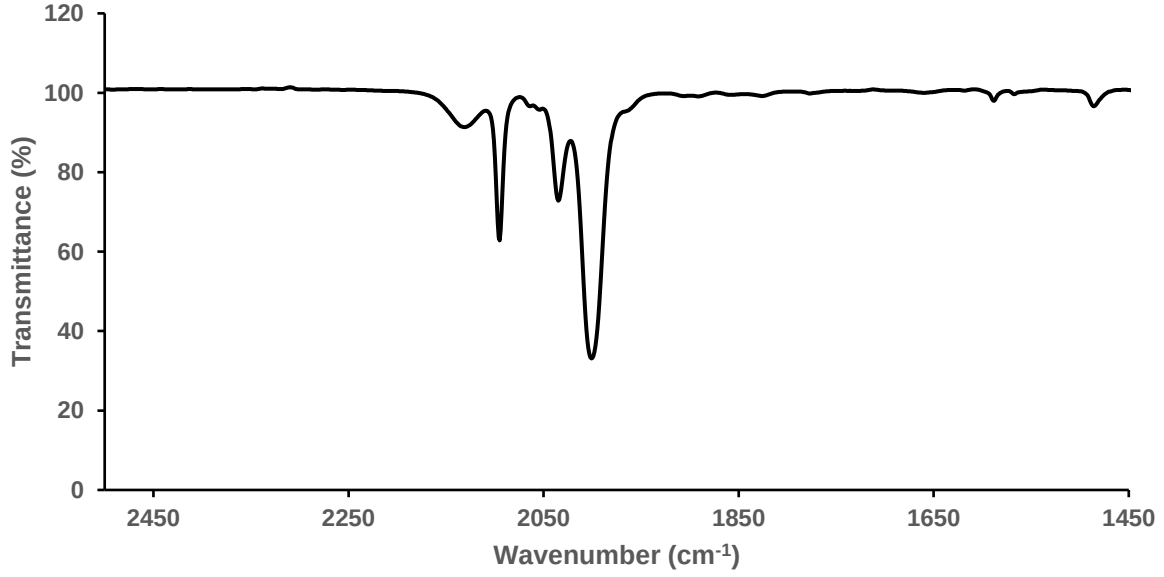

Figure A.3: Solution cell IR spectrum displaying the carbonyl stretching region of $Ph_3SiCo(CO)_4$ in CH_2Cl_2.

Appendix B – Crystal Structure Data

$[Co_2(CO)_6(BPP)_2][(PF_6)_2]$ CRYSTAL SUMMARY

Crystal data for $C_{38}H_{35}Cl_4CoF_6O_3P_3$; M_r = 947.30; Triclinic; space group P-1; *a* = 10.3098(8) Å; *b* = 11.0259(14) Å; *c* = 18.1444(14) Å; α = 91.316(3)°; β = 90.868(2)°; γ = 99.2265(17)°; V = 2035.0(3) $Å^3$; Z = 2; T = 120(2) K; λ(Mo-Kα) = 0.71073 Å; μ(Mo-Kα) = 0.867 mm^{-1}; d_{calc} = 1.546 $g.cm^{-3}$; 59825 reflections collected; 10148 unique (R_{int} = 0.0444); giving R_1 = 0.0734, wR_2 = 0.1990 for 9029 data with [I>2σ(I)] and R_1 = 0.0803, wR_2 = 0.2031 for all 10148 data. Residual electron density ($e^-.Å^{-3}$) max/min: 1.535/-2.196.

An arbitrary sphere of data was collected on a dark orange block-like crystal, having approximate dimensions of 0.221 × 0.199 × 0.168 mm, on a Bruker PHOTON-II diffractometer using a combination of ω- and φ-scans of 0.5° [1]. Data were corrected for absorption and polarization effects and analyzed for space group determination [2]. The structure was solved by dual-space methods and expanded routinely [3]. The model was refined by full-matrix least-squares analysis of F^2 against all reflections [4]. All non-hydrogen atoms were refined with anisotropic atomic displacement parameters. Unless otherwise noted, hydrogen atoms were included in calculated positions. Atomic displacement parameters for the hydrogens were tied to the equivalent isotropic displacement parameter of the atom to which they are bonded (U_{iso}(H) = 1.5U_{eq}(C) for methyl, 1.2U_{eq}(C) for all others).

REFERENCES

[1] *APEX-3*. Bruker AXS. Madison, Wisconsin, USA. **2016**.

[2] L. Krause, R. Herbst-Irmer, G. M. Sheldrick, & D. Stalke. *J. Appl. Cryst.* **2015** *48*, 3.

[3] G. M. Sheldrick. *Acta Cryst.*, **2015**, *A71*, 3.

[4] G. M. Sheldrick. *Acta Cryst.*, **2015**, *C71*, 3

Table B.1: Crystal data and structure refinement for $[Co_2(CO)_6(BPP)_2][(PF_6)_2]$

Empirical formula	$C_{38}H_{35}Cl_4CoF_6O_3P_3$
Formula weight	947.30
Temperature	120(2) K
Wavelength	0.71073 Å
Crystal system	Triclinic
Space group	P-1
Unit cell dimensions	*a* = 10.3098(8) Å
	b = 11.0259(14) Å
	c = 18.1444(14) Å
	α = 91.316(3)°
	β = 90.868(2)°
	γ = 99.2265(17)°
Volume	2035.0(3) $Å^3$
Z	2
Density (calculated)	1.546 $g.cm^{-3}$
Absorption coefficient (μ)	0.867 mm^{-1}
F(000)	962
Crystal color, habit	dark orange, block
Crystal size	0.221 × 0.199 × 0.168 mm^3
θ range for data collection	1.872 to 28.351°
Index ranges	-13 ≤ h ≤ 13, -14 ≤ k ≤ 14, -24 ≤ l ≤ 24
Reflections collected	59825
Independent reflections	10148 [R_{int} = 0.0444]
Completeness to θ = 25.242°	99.9 %
Absorption correction	Numerical
Max. and min. transmission	1.0000 and 0.6941
Refinement method	Full-matrix least-squares on F^2
Data / restraints / parameters	10148 / 0 / 496
Goodness-of-fit on F^2	1.111
Final R indices [I>2σ(I)]	R_1 = 0.0734, wR_2 = 0.1990
R indices (all data)	R_1 = 0.0803, wR_2 = 0.2031
Extinction coefficient	n/a
Largest diff. peak and hole	1.535 and -2.196 $e^-.Å^{-3}$

Table B.2: Bond lengths [Å] for $[Co_2(CO)_6(BPP)_2][(PF_6)_2]$.

atom-atom	distance	atom-atom	distance
Co(1)-C(3)	1.784(4)	Co(1)-C(2)	1.785(5)
Co(1)-C(1)	1.798(4)	Co(1)-P(1)	2.1848(10)
Co(1)-Co(1)#1	2.6732(10)	P(1)-C(6)	1.806(4)
P(1)-C(12)	1.826(4)	P(1)-C(4)	1.849(4)
P(2)-C(31)	1.792(4)	P(2)-C(25)	1.795(4)
P(2)-C(5)	1.805(4)	P(2)-C(18)	1.813(4)
O(1)-C(1)	1.146(6)	O(2)-C(2)	1.131(6)
O(3)-C(3)	1.142(5)	C(4)-C(5)	1.528(5)
C(4)-H(4A)	0.9900	C(4)-H(4B)	0.9900

C(5)-H(5A)	0.9900	C(5)-H(5B)	0.9900
C(6)-C(11)	1.402(6)	C(6)-C(7)	1.407(6)
C(7)-C(8)	1.383(7)	C(7)-H(7)	0.9500
C(8)-C(9)	1.386(7)	C(8)-H(8)	0.9500
C(9)-C(10)	1.388(7)	C(9)-H(9)	0.9500
C(10)-C(11)	1.390(6)	C(10)-H(10)	0.9500
C(11)-H(11)	0.9500	C(12)-C(13)	1.391(6)
C(12)-C(17)	1.401(6)	C(13)-C(14)	1.401(6)
C(13)-H(13)	0.9500	C(14)-C(15)	1.379(7)
C(14)-H(14)	0.9500	C(15)-C(16)	1.392(7)
C(15)-H(15)	0.9500	C(16)-C(17)	1.391(6)
C(16)-H(16)	0.9500	C(17)-H(17)	0.9500
C(18)-C(19)	1.517(5)	C(18)-H(18A)	0.9900
C(18)-H(18B)	0.9900	C(19)-C(24)	1.387(6)
C(19)-C(20)	1.393(6)	C(20)-C(21)	1.401(6)
C(20)-H(20)	0.9500	C(21)-C(22)	1.383(7)
C(21)-H(21)	0.9500	C(22)-C(23)	1.391(7)
C(22)-H(22)	0.9500	C(23)-C(24)	1.392(6)
C(23)-H(23)	0.9500	C(24)-H(24)	0.9500
C(25)-C(30)	1.399(6)	C(25)-C(26)	1.403(6)
C(26)-C(27)	1.386(6)	C(26)-H(26)	0.9500
C(27)-C(28)	1.388(7)	C(27)-H(27)	0.9500
C(28)-C(29)	1.384(7)	C(28)-H(28)	0.9500
C(29)-C(30)	1.393(6)	C(29)-H(29)	0.9500
C(30)-H(30)	0.9500	C(31)-C(36)	1.395(6)
C(31)-C(32)	1.397(6)	C(32)-C(33)	1.402(6)
C(32)-H(32)	0.9500	C(33)-C(34)	1.372(7)
C(33)-H(33)	0.9500	C(34)-C(35)	1.391(7)
C(34)-H(34)	0.9500	C(35)-C(36)	1.383(6)
C(35)-H(35)	0.9500	C(36)-H(36)	0.9500
Cl(1)-C(37)	1.748(6)	Cl(2)-C(37)	1.761(6)
C(37)-H(37A)	0.9900	C(37)-H(37B)	0.9900
Cl(3)-C(38)	1.694(8)	Cl(4)-C(38)	1.796(8)
C(38)-H(38A)	0.9900	C(38)-H(38B)	0.9900
P(3)-F(1)	1.585(3)	P(3)-F(6)	1.596(3)
P(3)-F(4)	1.604(3)	P(3)-F(2)	1.605(3)
P(3)-F(3)	1.609(3)	P(3)-F(5)	1.615(3)

Symmetry transformations used to generate equivalent atoms:

#1 -x+1,-y+1,-z

Table B.3: Bond angles [°] for $[Co_2(CO)_6(BPP)_2][(PF_6)_2]$.

atom-atom-atom	angle	atom-atom-atom	angle
C(3)-Co(1)-C(2)	123.1(2)	C(3)-Co(1)-C(1)	118.4(2)
C(2)-Co(1)-C(1)	116.8(2)	C(3)-Co(1)-P(1)	91.88(13)
C(2)-Co(1)-P(1)	96.20(13)	C(1)-Co(1)-P(1)	95.02(13)
C(3)-Co(1)-Co(1)#1	81.38(13)	C(2)-Co(1)-Co(1)#1	87.78(13)
C(1)-Co(1)-Co(1)#1	88.01(13)	P(1)-Co(1)-Co(1)#1	173.25(4)

C(6)-P(1)-C(12)	102.47(18)	C(6)-P(1)-C(4)	104.06(18)
C(12)-P(1)-C(4)	103.29(17)	C(6)-P(1)-Co(1)	113.57(13)
C(12)-P(1)-Co(1)	117.91(14)	C(4)-P(1)-Co(1)	113.88(13)
C(31)-P(2)-C(25)	107.96(18)	C(31)-P(2)-C(5)	109.80(18)
C(25)-P(2)-C(5)	107.48(19)	C(31)-P(2)-C(18)	108.83(19)
C(25)-P(2)-C(18)	111.44(19)	C(5)-P(2)-C(18)	111.27(19)
O(1)-C(1)-Co(1)	178.7(4)	O(2)-C(2)-Co(1)	177.9(4)
O(3)-C(3)-Co(1)	178.0(4)	C(5)-C(4)-P(1)	109.4(3)
C(5)-C(4)-H(4A)	109.8	P(1)-C(4)-H(4A)	109.8
C(5)-C(4)-H(4B)	109.8	P(1)-C(4)-H(4B)	109.8
H(4A)-C(4)-H(4B)	108.2	C(4)-C(5)-P(2)	115.6(3)
C(4)-C(5)-H(5A)	108.4	P(2)-C(5)-H(5A)	108.4
C(4)-C(5)-H(5B)	108.4	P(2)-C(5)-H(5B)	108.4
H(5A)-C(5)-H(5B)	107.4	C(11)-C(6)-C(7)	119.0(4)
C(11)-C(6)-P(1)	118.3(3)	C(7)-C(6)-P(1)	122.7(3)
C(8)-C(7)-C(6)	120.2(4)	C(8)-C(7)-H(7)	119.9
C(6)-C(7)-H(7)	119.9	C(7)-C(8)-C(9)	120.4(4)
C(7)-C(8)-H(8)	119.8	C(9)-C(8)-H(8)	119.8
C(8)-C(9)-C(10)	120.0(4)	C(8)-C(9)-H(9)	120.0
C(10)-C(9)-H(9)	120.0	C(9)-C(10)-C(11)	120.3(4)
C(9)-C(10)-H(10)	119.8	C(11)-C(10)-H(10)	119.8
C(10)-C(11)-C(6)	120.0(4)	C(10)-C(11)-H(11)	120.0
C(6)-C(11)-H(11)	120.0	C(13)-C(12)-C(17)	119.6(4)
C(13)-C(12)-P(1)	121.5(3)	C(17)-C(12)-P(1)	118.9(3)
C(12)-C(13)-C(14)	120.1(4)	C(12)-C(13)-H(13)	120.0
C(14)-C(13)-H(13)	120.0	C(15)-C(14)-C(13)	120.1(4)
C(15)-C(14)-H(14)	120.0	C(13)-C(14)-H(14)	120.0
C(14)-C(15)-C(16)	120.2(4)	C(14)-C(15)-H(15)	119.9
C(16)-C(15)-H(15)	119.9	C(17)-C(16)-C(15)	120.1(4)
C(17)-C(16)-H(16)	119.9	C(15)-C(16)-H(16)	119.9
C(16)-C(17)-C(12)	119.9(4)	C(16)-C(17)-H(17)	120.0
C(12)-C(17)-H(17)	120.0	C(19)-C(18)-P(2)	113.8(3)
C(19)-C(18)-H(18A)	108.8	P(2)-C(18)-H(18A)	108.8
C(19)-C(18)-H(18B)	108.8	P(2)-C(18)-H(18B)	108.8
H(18A)-C(18)-H(18B)	107.7	C(24)-C(19)-C(20)	119.6(4)
C(24)-C(19)-C(18)	120.2(4)	C(20)-C(19)-C(18)	120.1(4)
C(19)-C(20)-C(21)	119.8(4)	C(19)-C(20)-H(20)	120.1
C(21)-C(20)-H(20)	120.1	C(22)-C(21)-C(20)	120.5(4)
C(22)-C(21)-H(21)	119.7	C(20)-C(21)-H(21)	119.7
C(21)-C(22)-C(23)	119.4(4)	C(21)-C(22)-H(22)	120.3
C(23)-C(22)-H(22)	120.3	C(22)-C(23)-C(24)	120.4(4)
C(22)-C(23)-H(23)	119.8	C(24)-C(23)-H(23)	119.8
C(19)-C(24)-C(23)	120.3(4)	C(19)-C(24)-H(24)	119.9
C(23)-C(24)-H(24)	119.9	C(30)-C(25)-C(26)	120.0(4)
C(30)-C(25)-P(2)	117.5(3)	C(26)-C(25)-P(2)	122.4(3)
C(27)-C(26)-C(25)	119.4(4)	C(27)-C(26)-H(26)	120.3
C(25)-C(26)-H(26)	120.3	C(26)-C(27)-C(28)	120.5(4)
C(26)-C(27)-H(27)	119.7	C(28)-C(27)-H(27)	119.7
C(29)-C(28)-C(27)	120.3(4)	C(29)-C(28)-H(28)	119.9
C(27)-C(28)-H(28)	119.9	C(28)-C(29)-C(30)	120.1(4)
C(28)-C(29)-H(29)	119.9	C(30)-C(29)-H(29)	119.9

C(29)-C(30)-C(25)	119.7(4)	C(29)-C(30)-H(30)	120.2
C(25)-C(30)-H(30)	120.2	C(36)-C(31)-C(32)	120.0(4)
C(36)-C(31)-P(2)	118.1(3)	C(32)-C(31)-P(2)	121.6(3)
C(31)-C(32)-C(33)	119.2(4)	C(31)-C(32)-H(32)	120.4
C(33)-C(32)-H(32)	120.4	C(34)-C(33)-C(32)	120.5(4)
C(34)-C(33)-H(33)	119.8	C(32)-C(33)-H(33)	119.8
C(33)-C(34)-C(35)	120.2(4)	C(33)-C(34)-H(34)	119.9
C(35)-C(34)-H(34)	119.9	C(36)-C(35)-C(34)	120.3(4)
C(36)-C(35)-H(35)	119.9	C(34)-C(35)-H(35)	119.9
C(35)-C(36)-C(31)	119.9(4)	C(35)-C(36)-H(36)	120.1
C(31)-C(36)-H(36)	120.1	Cl(1)-C(37)-Cl(2)	112.2(3)
Cl(1)-C(37)-H(37A)	109.2	Cl(2)-C(37)-H(37A)	109.2
Cl(1)-C(37)-H(37B)	109.2	Cl(2)-C(37)-H(37B)	109.2
H(37A)-C(37)-H(37B)	107.9	Cl(3)-C(38)-Cl(4)	112.8(4)
Cl(3)-C(38)-H(38A)	109.0	Cl(4)-C(38)-H(38A)	109.0
Cl(3)-C(38)-H(38B)	109.0	Cl(4)-C(38)-H(38B)	109.0
H(38A)-C(38)-H(38B)	107.8	F(1)-P(3)-F(6)	91.24(19)
F(1)-P(3)-F(4)	91.25(17)	F(6)-P(3)-F(4)	90.26(16)
F(1)-P(3)-F(2)	89.82(17)	F(6)-P(3)-F(2)	89.76(16)
F(4)-P(3)-F(2)	178.93(17)	F(1)-P(3)-F(3)	179.1(2)
F(6)-P(3)-F(3)	89.63(18)	F(4)-P(3)-F(3)	89.07(16)
F(2)-P(3)-F(3)	89.86(16)	F(1)-P(3)-F(5)	90.1(2)
F(6)-P(3)-F(5)	178.57(19)	F(4)-P(3)-F(5)	90.09(16)
F(2)-P(3)-F(5)	89.88(15)	F(3)-P(3)-F(5)	89.00(18)

Symmetry transformations used to generate equivalent atoms:

#1 -x+1,-y+1,-z